Journal of Hydrology 528 (2015) 161–176

Contents lists available at ScienceDirect

Journal of Hydrology

journal homepage: www.elsevier.com/locate/jhydrol

# The dissolved chemical and isotopic signature downflow the confluence of two large rivers: The case of the Parana and Paraguay rivers

Verena Agustina Campodonico *, María Gabriela García, Andrea Inés Pasquini

*Centro de Investigaciones en Ciencias de la Tierra (CICTERRA), Consejo Nacional de Investigaciones Científicas y Técnicas (CONICET) y Universidad Nacional de Córdoba, Av. Vélez Sarsfield 1611, X5016CGA Córdoba, Argentina*

ARTICLE INFO

*Article history:*
Received 5 May 2014
Received in revised form 27 April 2015
Accepted 13 June 2015
Available online 17 June 2015
This manuscript was handled by Laurent Charlet, Editor-in-Chief, with the assistance of Prosun Bhattacharya, Associate Editor

*Keywords:*
Middle Paraná River
South American large rivers
Mixing of waters
Mass balance model
Water isotopes
Hydrochemistry

SUMMARY

The Paraná River basin is one of the largest hydrological systems in South America (~$2.6 \times 10^6$ km$^2$). Downflow the confluence of tributaries, most large rivers exhibit transverse and longitudinal inhomogeneities that can be detected for tens or even hundreds of kilometers. Concordantly, a noticeable cross-sectional chemical asymmetry in the dissolved load was distinguished in the Middle Paraná River, after the confluence of its main tributaries (i.e., the Paraguay and Upper Paraná rivers). Water chemistry and isotopic signature in three cross-sections along the Middle Paraná River, as well as from main and minor tributaries, and some deep (~105 m bs) and shallow boreholes (~15 m bs) located near both river banks, were analyzed in order to define the extent of mixing and identify possible contributions from groundwater discharges. Downflow the confluence of the Upper Paraná and Paraguay rivers a chemical and isotopic asymmetry was observed, mainly through the values of EC, major ions ($Ca^{2+}$, $Na^+$, $Mg^{2+}$, $Cl^-$ and $SO_4^{2-}$), some trace elements (Fe, U, Th, Ba, Sr, As and REE) and stable isotopes ($\delta^{18}O$ and $\delta^2H$). Toward its western margin, higher elemental concentrations which resembled that of the Paraguay River were measured, whereas at the eastern border, waters were more diluted and preserved the chemical signature of the Upper Paraná River. This variability remained detectable at least until ~225 km downflow the confluence, where differences between western and eastern margins were less evident. At ~580 km downflow the confluence, a slight inversion in the transverse chemical asymmetry was observed. This trend switch can be the result of the input of solutes from minor tributaries that reach the main channel from the East and/or may be due to higher groundwater discharges from the East bank. A mass balance model was applied, as a first approach, to estimate the groundwater inflow using the geochemical tracer $^{222}Rn$. The results indicate that groundwater contributions represent between ~0.5% and 6% of the total water inputs to the Middle Paraná River under baseflow conditions. This implies that the chemical asymmetry in the Middle Parana River is mostly due to the incomplete mixing of the main tributaries. Though the influence of groundwater is not a determining factor in the chemical variability of the river, it may partially explain the higher concentrations of some trace elements found in the eastern margin ~580 km downflow the confluence.



## 1. Introduction

Large rivers play a significant role in continental denudation as they transport the erosion products from the continents to the oceans. Potter (1978) considered that area of drainage basin, river length, volume of transported sediments and water discharge are the four main characteristics that define a large river, and used the first two to identify the 50 largest rivers of the world. Later, Meade (1996) listed the 25 rivers that present the largest discharges of water and suspended sediments to the world oceans. Recently, Milliman and Farnsworth (2011) published an extensive data base containing global rivers discharge and sediments fluxes from the continents to the oceans, and listed 12 rivers that account for ~25% of the total continental areas draining into the world oceans, and discharge ~35% of the freshwater reaching the ocean.

In South America, the large rivers Amazonas, Orinoco and Paraná are responsible for the greatest discharge of freshwater (i.e., ~8000 m$^3$ yr$^{-1}$) into the Atlantic Ocean (Milliman and Farnsworth, 2011). In turn, Tundisi (1994) pointed out that these three rivers supply about 13% of the total suspended solids delivered by all world rivers to the oceans (i.e., 570 Mt yr$^{-1}$, Milliman and Farnsworth, 2011).

The Paraná River is about 4000 km long and its drainage basin, the second largest in South America, has an area of $2.6 \times 10^6$ km$^2$

* Corresponding author. Tel.: +54 (0) 351 5353800x30228.
*E-mail address:* vcampodonico@efn.uncor.edu (V.A. Campodonico).

http://dx.doi.org/10.1016/j.jhydrol.2015.06.027
0022-1694/

(Orfeo and Stevaux, 2002). Its average annual discharge is about 17,000 $m^3 s^{-1}$ (Pasquini and Depetris, 2007) and on the average it delivers 530 $km^3 yr^{-1}$ of water to the Río de la Plata estuary (Pasquini and Depetris, 2010). The Paraná River transports $6.2 \times 10^4$ t $yr^{-1}$ of dissolved load and $9 \times 10^7$ t $yr^{-1}$ of total suspended solids to the Atlantic Ocean (Milliman and Farnsworth, 2011).

Most large rivers exhibit inhomogeneities in four dimensions: longitudinal (i.e., downstream), transverse, vertical and temporal. The first two, are frequent features observed downflow the confluence with tributaries, where parallel water bodies can be distinguished (Yang et al., 1996). A number of methods have been used to study these inhomogeneities. For example, remotely sensed data (i.e., airborne and satellite multispectral images) were used to study the visual mixing downflow the confluence of two large rivers (e.g., Lane et al., 2008; Matsui et al., 1976). Chemical tools include the use of dye tracers (e.g., Caplow et al., 2004) and surveys of naturally occurring dissolved chemical compounds (e.g., Leibundgut et al., 2009).

Several studies reported field data showing a transverse chemical asymmetry in large rivers. For instance, Pawellek (1995) identified a chemical asymmetry in the Danube River due to the incomplete mixing of the Iller and Lech rivers, and established that once the volume of the main course exceeded that of its tributaries by a factor of 10–15, the chemical composition became homogenous. Transverse chemical variations in the Amazon River were reported by Aucour et al. (2003) downflow the confluence of the Negro and Solimões rivers, using major elements and organic carbon concentrations. A few kilometers upstream this confluence, Bouchez et al. (2010) also found cross-sectional heterogeneities in the confluence of the Purús and Solimões rivers. Lateral chemical and isotopic heterogeneities are also caused by groundwater discharges, as it was determined at the confluence of the Garonne and Ariège rivers in the SW of France, as well as in the confluence of the Ganges and Yamuna rivers in northern India (Lambs, 2004).

Drago and Vassallo (1980) first reported a noticeable cross-sectional chemical asymmetry in the middle stretch of the Paraná River that was recognized up to ~200 km downstream the confluence of its main tributaries, i.e. the Paraguay and Upper Paraná rivers. Based only on data from major dissolved composition, these authors found that water flowing near the western margin was saltier than water from the eastern border, and attributed this behavior to the influence of the tributaries that imparted their own chemical signatures. Furthermore, on the basis of remote sensing images, Lane et al. (2008) determined that the mixing length in the Middle Paraná River varied between 8 and 400 km.

The goal of this paper is to identify the factors that control the transverse chemical asymmetry detected in the Middle Paraná River downflow the confluence of the Paraguay and Upper Paraná rivers, using new evidences that include major and trace dissolved components and isotopic tracers ($\delta^{18}O$, $\delta^{2}H$ and $^{222}Rn$). In addition, the inputs of water from the different hydrological compartments that interact in this river stretch were quantified using a model based on $^{222}Rn$ mass-balance.

## 2. Study area

The Paraná River drainage basin (Fig. 1) constitutes one of the largest in South America. It covers an area of about $2.6 \times 10^6$ $km^2$ (Orfeo and Stevaux, 2002) and supplies about 80% of the total discharge of the Río de la Plata. Its northernmost water sources, at the

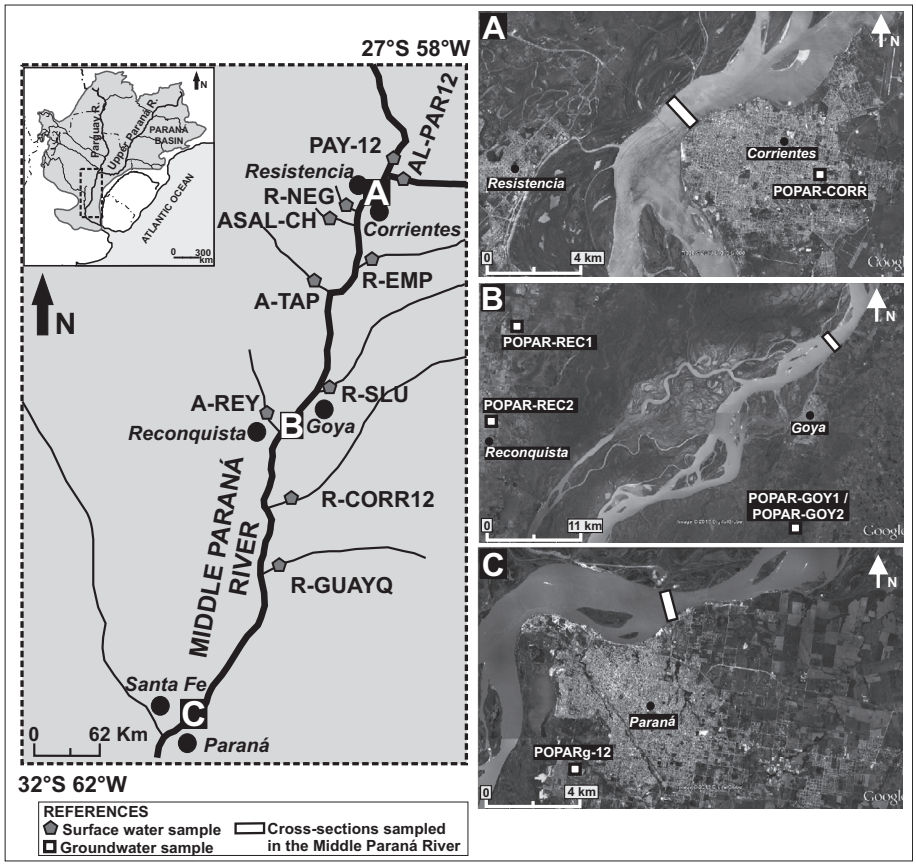


**Fig. 1.** Map of the Middle Paraná drainage basin showing the location of surface and groundwater sampling sites. Cross-section A: Corrientes–Resistencia (27°27′35″S); Cross-section B: Goya–Reconquista (29°03′45″S); and Cross-section C: Paraná–Santa Fe (31°42′10″S). The sampling station names are indicated in Table 1.

Upper Paraná River headwaters, are placed at Serra dos Preneos (~45°W), close to the Atlantic coast in Brazil. With headwaters at the Gran Pantanal, one of the largest wetlands in the world (Mato Grosso and Mato Grosso do Sul states, Brazil, ~15°S and ~55–60°W), the Paraguay River joins the Upper Paraná River near the city of Corrientes (Fig. 1). A few kilometers upstream the confluence, the Paraguay River receives the contributions of the Pilcomayo and Bermejo rivers, whose headwaters are located at the Andes foothills (in western Argentina and Bolivia, ~65°W). The stretch encompassed between the confluence of Paraguay and Upper Paraná rivers and the city of Diamante (32°04′11″S 60°38′16″W; Entre Ríos province, Argentina), located ~600 km downflow the confluence, is known as Middle Paraná River (Drago and Vassallo, 1980). The floodplain in this stretch is dissected by river channels, shallow lakes, islands, and wetlands. Average water discharge of the Middle Paraná River (mean for September 2009–August 2012) is about 20,250 $m^3 s^{-1}$ at the city of Corrientes (Argentina's Subsecretaría de Recursos Hídricos, www.hidricosargentina.gov.ar). Maximum annual discharge in the Paraná (Fig. 2A), Bermejo and Pilcomayo rivers occurs during the austral summer (February–March), whereas the Paraguay River reaches maximum flow in June (austral winter, Pasquini and Depetris, 2007). The main contributor to the Middle Paraná River discharge is the Upper Paraná River (i.e., including the Iguaçu River), which supplies ~73% of the riverine water budget, whereas the Paraguay River delivers ~27% of the total water budget (Fig. 2B; Pasquini and Depetris, 2007). In contrast to what occurs with the flow, most of the sediment load in the Middle Paraná comes from the Paraguay River, which supplies ~92% of the total load (i.e., including the Bermejo and Pilcomayo rivers contribution), whereas the remaining 8% is delivered by the Upper Paraná River. Amsler and Drago (2009) estimated a suspended sediment load of ~$1.2 \times 10^8$ t $yr^{-1}$ for the Middle Paraná River during the 1990s. Depetris and Griffin (1968) determined the mineralogy of the <2 μm size fraction of the suspended sediment load in the Paraná's lowermost reaches. They found that illite was the most abundant phase, followed by smectite > kaolinite > chlorite. The coarser size fraction (2–20 μm) was mainly composed by K-feldspar, plagioclase, mica and quartz, indicating that acid igneous and crystalline basement rocks are the main source.

The summer circulation over South America is dominated by a monsoonal system, whose major seasonal feature during austral summer is the South Atlantic Convergence Zone (SACZ), placed along the north-eastern boundary of the Río de la Plata drainage basin (e.g., Garreaud et al., 2008). Another significant feature in the regional climatic control is a low-level northerly/northeasterly jet that flows east of the Andes, and delivers moisture along the corridor placed between the Andes ranges and the Brazilian *altiplano* (e.g., Wang and Fu, 2004). As a consequence of these continental climatic features, mean annual rainfall is unevenly distributed along the Paraná basin. Maximum precipitation (2400 mm $yr^{-1}$) occurs along the eastern margin of the basin, whereas toward the west, along the 60–65°W strip, rainfall decreases to 400–800 mm $yr^{-1}$ (Pasquini and Depetris, 2007). Mean temperatures in January (austral summer) are between 20 and 30 °C in the whole basin, while in July (austral winter) mean

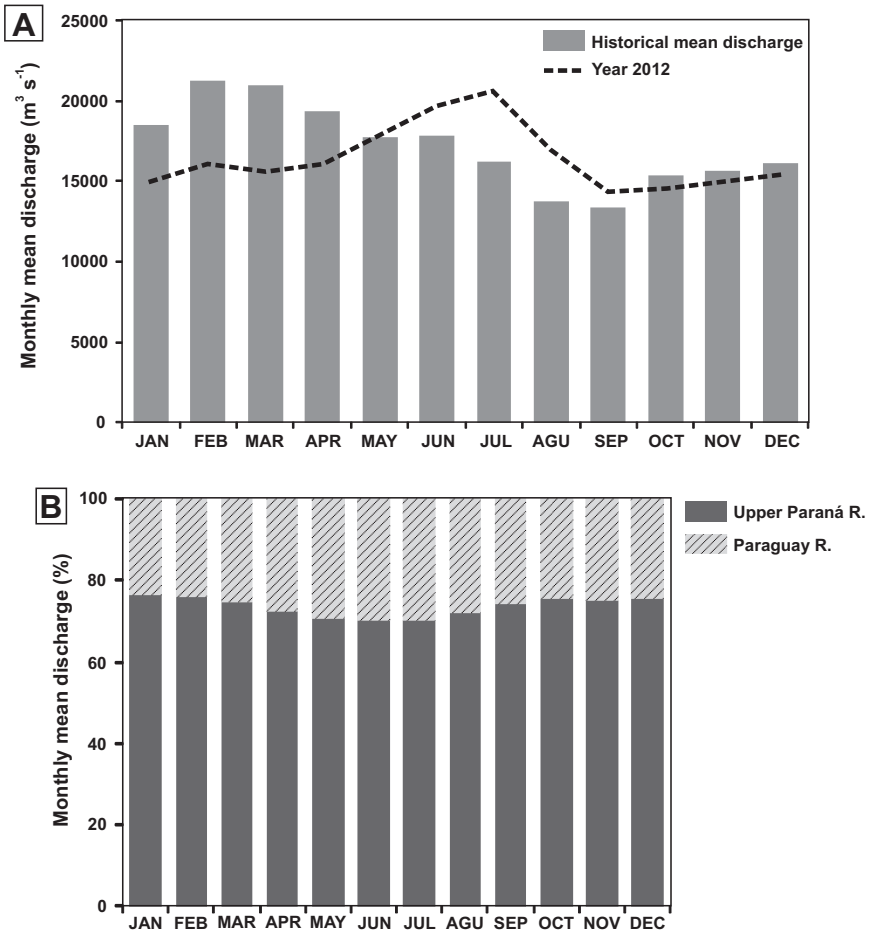


**Fig. 2.** (A) Hydrograph of the Middle Paraná River at Corrientes gauging station. Historical data series correspond to the period 1904–2012. The dashed line corresponds to the monthly mean discharge in the sampling year. (B) Relative contributions of tributaries to the Middle Paraná River discharge at Corrientes station.

temperatures are between 15 and 25 °C in the northern and center portions of the basin, and range from 10 to 15 °C in the South. Natural factors and also human activities (i.e., directly, through dams or, indirectly, through the use of the land) may affect the hydrological functioning of river basins. The Upper Paraná River, for example, has in operation many reservoir dams (about 130) (Ravenga et al., 1998), which regulate its discharge and control sediment fluxes. Neither the Paraguay nor its tributaries have major dams in their respective headwaters.

The stratigraphy of the study area is characterized by a succession of sedimentary formations known in Argentina as Chacoparanaense basin (Fig. 3). Some of them host important aquifers, the most relevant being the Guarani Aquifer System ($\sim 1.2 \times 10^6$ km$^2$, Araujo et al., 1999). The hydrogeological basement consists of diverse Permo–Triassic sedimentary rocks, which also form an aquitard, and are known as Rio do Rasto Formation in Brazil and as Victorino Rodrigues Formation in Argentina (Araujo et al., 1999). This unit is composed of very fine to fine sandstones, mudstones and siltstones (Bonotto, 2006). The Permian-Cretaceous Guarani Aquifer, *a.k.a.* Mercosul Aquifer (Araujo et al., 1999), has an average thickness of 300–400 m. It is composed by the Piram bóia–Botucatu succession, which comprises sandstones and sandy-siltstones (Donatti et al., 2001). The Botucatu eolian system overlies the fluvio-eolian deposits of the Pirambóia system. This sedimentary succession is known as Buena Vista–Tacuarembó in Argentina. The confining layer overlying this aquifer is composed of thick Cretaceous basalts of the Serra Geral Formation (up to 1500 m) (e.g., Bonotto and Caprioglio, 2002). The red sandstones of the Cretaceous Bauru Group (average thickness of 100 m) exhibit adequate properties to store water (Bonotto, 2006), and can be found in some parts of the basin overlying the basalts (Fernandes and Coimbra, 1996). The Cenozoic aquifer systems in Argentina include the Paraná and Ituzaingó formations, as well as some recent alluvial deposits. The Miocene Paraná Formation includes marine, fine to medium grained-sized sandstones interbedded with green shales (e.g., Fili, 2001). The Ituzaingó Formation, *a.k.a.* Puelches Formation at Santa Fe and Buenos Aires provinces (Pliocene–Pleistocene), is made of fine and medium quartzitic fluvial sandstones interbedded with siltstones (e.g., Diaz et al., 2009). The Toropí–Yupoí Formations (Upper Pleistocene) are found above the Ituzaingó Formation at Corrientes province, and are composed of sandstones interbedded with silty and clayed lenses. A wide variety of shallow aquifers cover the watershed. Thereby, at Santa Fe province for example, the uppermost aquifers consist of alluvial sediments deposited by the Paraná River and are composed of sands interbedded with silts and clays, while others, known as Transition to Puelches Aquifer are composed of silty sandstones (Auge, 2004).

## 3. Materials and methods

### 3.1. Sampling and analyses

Surface and groundwater samples were collected from rivers and wells in the Middle Paraná River basin (Fig. 1, Table 1). The main river channel was sampled along three cross-sections located from North to South at: (A) Resistencia–Corrientes (27°27′35″S), (B) Reconquista–Goya (29°03′45″S), and (C) Santa Fe–Paraná (31°42′10″S). Five sampling stations were set approximately equidistant in each cross-section. At each sampling point, two samples were taken at different depths in the water column: one at ~15 cm below the water surface, and the remaining at the average depth between the surface and the bed channel. The Paraguay and Upper Paraná rivers as well as minor tributaries draining downstream the confluence were also sampled, whereas groundwater samples were taken from available domestic and public wells drilled near both river banks (Fig. 1, Table 1). These samples were retrieved from the Toropí–Yupoí, Transition to Puelches, Ituzaingó and Paraná aquifers.

Sampling was carried out in November 2012, when baseflow conditions prevailed (Fig. 2A). The latter ensures a better identification of potential contributions from groundwater discharges and minimizes the effect of dilution caused by rainfall.

Field determinations consisted of pH, electrical conductivity (EC), total dissolved solids (TDS), temperature, oxidation reduction potential (ORP), and alkalinity measurements. Determinations

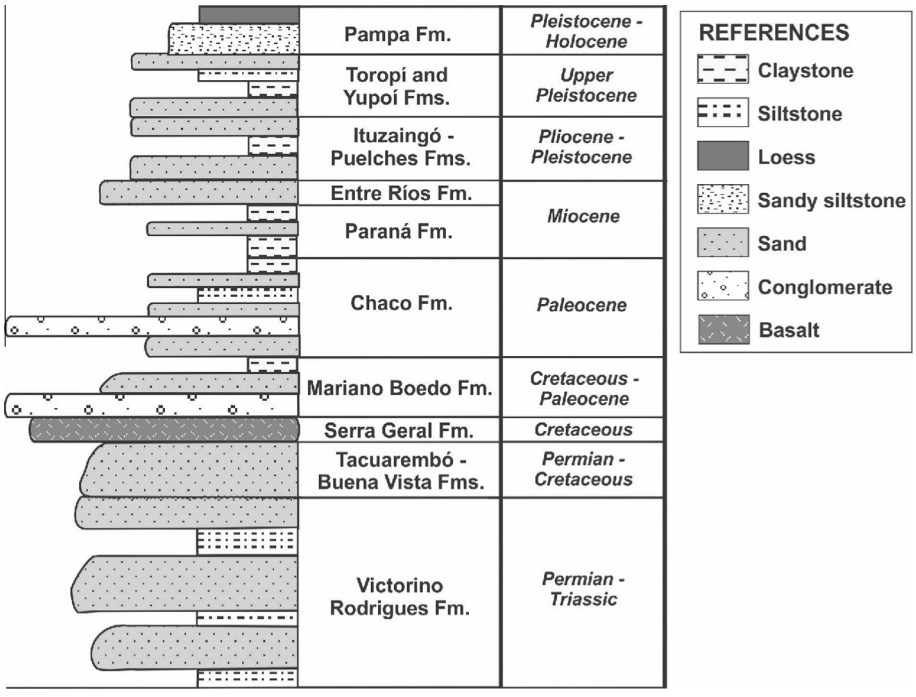


**Fig. 3.** Schematic stratigraphic column of the Chacoparanaense basin.

**Table 1**
Location, phisyco-chemical parameters, major ions, selected trace elements and stable isotopes of the samples taken at the Middle Paraná River, its tributaries and aquifers. The ORP values were adjusted with respect to hydrogen electrode and expressed as Eh.

| River/aquifer | Sample no. | Location | | Physico-chemical parameters | | | Major ions | | | | | | | | | Trace elements | | | | | | Stable isotopes | |
|---|---|---|---|---|---|---|---|---|---|---|---|---|---|---|---|---|---|---|---|---|---|---|---|
| | | Latitude | Longitude | EC | pH | Eh | $Ca^{2+}$ | $Na^{+}$ | $Mg^{2+}$ | $K^{+}$ | $Cl^{-}$ | $SO_4^{2-}$ | $NO_3^{-}$ | $HCO_3^{-}$ | Error | Fe | U | Th | Ba | Sr | As | $\delta^{18}O$ | $\delta^{2}H$ |
| | | S | W | $\mu S\ cm^{-1}$ | | mV | $mg\ L^{-1}$ | | | | | | | | % | $\mu g\ L^{-1}$ | | | | | | ‰ | |
| Middle | PARC2-11 | 27°27′43.6″ | 58°50′41.5″ | 73.0 | 7.0 | 379 | 5.0 | 6.3 | 2.2 | 2.4 | 7.9 | 1.2 | nd. | 24.4 | 8.3 | 80 | 0.02 | 0.003 | 32.8 | 36.4 | 0.25 | −4.1 | −25 |
| Paraná R. | PARC2−21 | 27°27′40.4″ | 58°50′49.6″ | 67.8 | 7.2 | 352 | 5.1 | 4.4 | 2.1 | 2.1 | 6.9 | 2.1 | 1.3 | 19.5 | 7.2 | 90 | 0.02 | 0.003 | 31.3 | 36.4 | 0.22 | −4.1 | −24 |
| Cross-section A | PARC2-31 | 27°27′30.8″ | 58°50′51.0″ | 93.7 | 7.2 | 391 | 6.6 | 8.4 | 2.5 | 2.7 | 11.8 | 3.6 | 1.6 | 30.5 | 1.7 | 200 | 0.06 | 0.009 | 34.9 | 49.4 | 0.51 | −3.6 | −20 |
| | PARC2-41 | 27°27′19.6″ | 58°51′2.2″ | 109.3 | 7.3 | 399 | 7.2 | 10.1 | 2.8 | 2.4 | 13.4 | 4.9 | 3.4 | 25.6 | 6.5 | 240 | 0.09 | 0.012 | 38.6 | 55.0 | 0.69 | −3.4 | −18 |
| | PARC2-51 | 27°27′4.3″ | 58°51′12.7″ | 150.5 | 7.2 | 418 | 8.2 | 14.6 | 3.4 | 2.5 | 20.5 | 7.1 | 3.2 | 25.6 | 7.3 | 390 | 0.12 | 0.023 | 56.8 | 53.9 | 1.08 | −2.7 | −13 |
| Middle | PARG2-11 | 29°3′58.5″ | 59°13′12.2″ | 71.3 | 7.2 | 388 | 5.0 | 5.7 | 2.3 | 2.1 | 9.6 | 2.8 | nd. | 20.7 | 5.2 | 150 | 0.04 | 0.007 | 44.5 | 34.0 | 0.47 | −4.6 | −24 |
| Paraná R. | PARG2-21 | 29°3′51.7″ | 59°13′18.4″ | 73.9 | 7.2 | 375 | 4.8 | 5.8 | 2.3 | 2.0 | nd. | 2.9 | nd. | 16.1 | 5.1 | 160 | 0.04 | 0.008 | 44.0 | 34.3 | 0.48 | −4.3 | −22 |
| Cross-section B | PARG2-31 | 29°3′45.5″ | 59°13′33.2″ | 82.6 | 7.2 | 390 | 5.4 | 6.6 | 2.3 | 2.1 | 8.8 | 3.0 | 1.7 | 22.3 | 6.5 | 210 | 0.05 | 0.012 | 47.0 | 38.2 | 0.58 | −3.9 | −21 |
| | PARG2-41 | 29°3′26.2″ | 59°13′44.3″ | 86.6 | 7.2 | 367 | 5.6 | 7.2 | 2.4 | 2.2 | 12.0 | 3.6 | 1.3 | 25.4 | −8.0 | 250 | 0.05 | 0.01 | 47.2 | 41.4 | 0.66 | −3.7 | −20 |
| | PARG2-51 | 29°3′15.5″ | 59°13′54.0″ | 88.9 | 7.4 | 392 | 6.0 | 7.9 | 2.5 | 2.5 | 11.9 | 3.9 | 2.3 | 23.5 | 4.5 | 280 | 0.06 | 0.016 | 50.9 | 45.1 | 0.67 | −3.8 | −20 |
| Middle | PARP2-11 | 31°42′32.3″ | 60°30′15.3″ | 85.8 | 7.2 | 375 | 5.7 | 7.6 | 2.3 | 2.1 | 12.6 | 4.5 | nd. | 23.4 | 1.6 | 230 | 0.08 | 0.014 | 47.8 | 45.4 | 0.73 | −3.7 | −21 |
| Paraná R. | PARP2-21 | 31°42′25.4″ | 60°30′18.2″ | 92.7 | 7.2 | 379 | 5.8 | 7.6 | 2.5 | 2.2 | 12.4 | 4.3 | 1.4 | 22.4 | 2.8 | 230 | 0.07 | 0.014 | 50.5 | 47.4 | 0.71 | −3.8 | −22 |
| Cross-section C | PARP2−31 | 31°42′15.3″ | 60°30′16.6″ | 85.7 | 7.1 | 402 | 5.7 | 7.7 | 2.3 | 2.1 | 12.4 | 4.3 | 1.4 | 23.1 | 1.1 | 250 | 0.07 | 0.014 | 37.1 | 45.6 | 0.64 | −3.5 | −21 |
| | PARP2-41 | 31°42′2.6″ | 60°30′13.3″ | 92.5 | 7.2 | 405 | 5.5 | 7.5 | 2.2 | 2.3 | 11.9 | 4.3 | 1.2 | 24.6 | −0.4 | 220 | 0.06 | 0.013 | 36.7 | 45.9 | 0.64 | −3.5 | −21 |
| | PARP2-51 | 31°41′52.6″ | 60°30′16.2″ | 89.0 | 7.1 | 389 | 5.6 | 7.6 | 2.3 | 2.1 | 12.6 | 4.5 | 2.2 | 24.8 | −2.3 | 210 | 0.06 | 0.011 | 36.6 | 46.4 | 0.65 | −3.6 | −21 |
| Paraguay R. | PAY-12 | 27°16′19.1″ | 58°35′48.5″ | 162.0 | 6.8 | 408 | 9.1 | 15.4 | 3.2 | 3.2 | 23.5 | 8.5 | 7.0 | 10.4 | −8.2 | 240 | 0.13 | 0.009 | 45.0 | 74.5 | 1.05 | −2.4 | −10 |
| Upper Paraná R. | ALPAR-12 | 27°17′03.9″ | 58°31′45.9″ | 68.7 | 7.1 | 386 | 4.1 | 4.5 | 1.7 | 1.3 | 5.7 | 1.8 | 2.5 | 25.6 | −6.7 | 60 | 0.01 | 0.001 | 24.2 | 30.0 | 0.20 | −4.4 | −25 |
| Empedrado R. | R-EMP | 27°52′03.5″ | 58°45′46.5″ | 242.0 | 7.4 | 388 | 15.8 | 22.5 | 4.7 | 8.3 | 33.1 | 11.7 | 4.1 | 46.4 | 8.3 | 510 | 0.31 | 0.033 | 89.1 | 170.0 | 6.45 | 0.8 | 10 |
| Corrientes R. | R-CORR12 | 29°48′37.2″ | 59°23′32.7″ | 259.0 | 7.2 | 379 | 12.0 | 30.1 | 3.4 | 1.4 | 58.5 | 15.0 | nd. | 24.3 | −3.1 | 300 | 0.20 | 0.029 | 42.8 | 121.0 | 1.92 | 1.2 | 12 |
| Santa Lucía R. | R-SLU | 29°05′40.5″ | 59°12′44.7″ | 436.0 | 7.7 | 398 | 19.4 | 73.0 | 5.6 | 5.4 | 85.3 | 31.7 | nd. | 54.9 | 8.8 | 60 | 0.89 | 0.004 | 85.3 | >200 | 4.57 | 0.3 | 7 |
| Guayquiraró R. | R-GUAYQ | 30°20′37.4″ | 59°30′49.3″ | 323.0 | 7.3 | 398 | 14.3 | 46.5 | 3.6 | 2.5 | 57.5 | 22.6 | 1.6 | 57.3 | 0.6 | 260 | 0.43 | 0.015 | 48.9 | 181.0 | 3.27 | 1.4 | 13 |
| Salado R. | ASAL-CH | 27°32′29.2″ | 59°07′48.1″ | 259.0 | 7.4 | 410 | 8.5 | 27.9 | 3.5 | 7.4 | 32.3 | 29.4 | 16.4 | 35.8 | −1.8 | 990 | 0.23 | 0.09 | 33.4 | 98.0 | 5.43 | 0 | 10 |
| Negro R. | R-NEG | 27°27′38.0″ | 58°54′42.0″ | 2920.0 | 7.7 | 394 | 14.8 | 110.6 | 47.5 | 9.5 | 132.4 | 107.6 | 4.7 | 131.2 | −0.3 | 110 | 0.55 | 0.004 | 139.0 | >200 | 5.16 | −1.6 | −3 |
| Tapenagá R. | A-TAP | 28°01′40.9″ | 59°13′30.8″ | 386.0 | 7.3 | 415 | 15.1 | 51.9 | 4.6 | 7.8 | 41.0 | 39.2 | 16.6 | 47.8 | 1.9 | 510 | 0.29 | 0.051 | 57.9 | 145.0 | 6.65 | −0.1 | 6 |
| El Rey R. | A-REY | 29°07′56.6″ | 59°39′05.9″ | 602.0 | 7.2 | 392 | 11.9 | 81.5 | 6.1 | 6.5 | 105.2 | 82.4 | 7.7 | 51.2 | −8.1 | 1070 | 0.50 | 0.086 | 63.6 | 131.0 | 5.12 | −3.1 | −13 |
| Toropí–Yupoí Aq. | POPAR-GOY1 | 29°16′28.0″ | 59°15′30.8″ | 369.0 | 7.1 | 395 | 25.1 | 41.3 | 4.3 | 5.2 | 20.6 | 8.8 | 5.6 | 136.6 | 6.6 | 30 | 3.93 | 0.001 | 147.0 | >200 | 3.02 | −5.5 | −30 |
| Transition to | POPAR-REC1 | 29°03′38.5″ | 59°37′04.3″ | 780.0 | 7.0 | 278 | 20.0 | 29.7 | 18.8 | 5.4 | 26.8 | 143.4 | nd. | 352.6 | −4.2 | 280 | 21.30 | 0.001 | 239.0 | >200 | 18.20 | −5.9 | −34 |
| Puelches Aq. | POPAR-REC2 | 29°09′36.7″ | 59°38′19.5″ | 932.0 | 6.9 | 237 | 43.9 | 53.3 | 33.7 | 6.6 | 48.0 | 25.1 | 3.8 | 329.4 | 0.7 | 390 | 1.36 | <0.001 | 319.0 | >200 | 3.65 | −4.8 | −26 |
| Ituzaingó Aq. | POPAR-CORR | 27°29′07.4″ | 58°47′1.8″ | 204.0 | 5.9 | 389 | 6.3 | 18.8 | 2.7 | 5.8 | 24.0 | 9.7 | 6.1 | 18.3 | 8.2 | 50 | 0.03 | <0.001 | 71.3 | 91.2 | 0.22 | −5.3 | −30 |
| | POPAR-GOY2 | 29°16′28.0″ | 59°15′30.8″ | 184.5 | 6.4 | 279 | 10.9 | 16.9 | 2.9 | 3.9 | 9.8 | 2.7 | 1.5 | 62.2 | 6.3 | 2270 | 0.06 | <0.001 | 121.0 | 130.0 | 0.14 | −5.4 | −33 |
| Paraná Aq. | POPARg-12 | 31°46′15.2″ | 60°32′57.5″ | 1830.0 | 7.1 | 394 | 19.5 | 360.4 | 14.2 | 7.3 | 110.6 | 210.7 | 159.0 | 444.1 | 1.8 | 20 | 16.60 | <0.001 | 36.7 | >200 | 39.60 | | |

were performed using standardized methods according to Eaton et al. (1995). The pH was measured using a Metrohm 827 portable pH-meter with a combined electrode and integrated NTC temperature sensor for automatic temperature compensation. ORP was determined with a Combined Pt-ring electrode that contains a Ag/AgCl internal reference electrode. The ORP values were adjusted with respect to hydrogen electrode and expressed as Eh. Electrical conductivity (EC) was measured using a Hach portable conductivity meter, and alkalinity was determined in 100 ml samples by titration using 0.16 N $H_2SO_4$ and bromocresol green-methyl red as end point indicator (Hach Co).

After collection, samples were filtered through 0.22 μm cellulose acetate membrane filters (Millipore Corp.) and divided into two aliquots. The filtration equipment was repeatedly rinsed with sample water prior to filtration. Aliquots used for major cations and trace elements determination (15 ml) were acidified to pH < 2 with ultrapure $HNO_3$ (>99.999%, redistilled, Aldrich Chemical) and stored in pre-cleaned polyethylene bottles. The remaining 20 ml aliquot was stored in polyethylene bottles, without acidifying, at 4 °C for the determination of major anions. Unfiltered samples were stored in 500 ml polyethylene bottles at 4 °C, for stable isotopes determinations.

Anions ($Cl^-$, $NO_3^-$, and $SO_4^{2-}$) were determined by chemically suppressed ion chromatography with conductivity detection, while cations and trace elements were measured by ICP-MS (Perkin Elmer Sciex Elan 6000 – quadrupole mass spectrometer). The validity of the results for major and trace elements were checked with NIST-1643e (Trace Elements in Water Reference Material certified by the National Institute of Standards & Technology, USA) and SRLS-5 (River Water Reference Material for Trace Metals certified by the National Research Council of Canada), carried out along with sample analysis. The accuracy of standard measures ranged between 1% and 10% in both cases. In addition, duplicated analysis were performed every 10 samples in order to check the reproducibility of results, and the precision ranged between 1% and 8% in all analyzed elements. For most of the analyzed waters, the charge imbalance between major cations and anions was less than 10%.

Stable isotopes $^2H$ and $^{18}O$ were measured using laser spectroscopy (OA-ICOS: Off-Axis Integrated Cavity Output Spectroscopy). Results are expressed as $\delta$‰ according to Eq. (1):

$$\delta\ (‰) = \frac{1000R_S - R_{V\text{-}SMOW}}{R_{V\text{-}SMOW}} \quad (1)$$

where $\delta$: isotopic deviation in ‰; $R$: isotopic ratio ($^2H/H$ or $^{18}O/^{16}O$); s: sample; and V-SMOW: reference material (Vienna Standard Mean Ocean Water, Gonfiantini, 1978). The analytical uncertainties are ±0.3‰ for $\delta^{18}O$ and ±1.0‰ for $\delta^2H$.

### 3.2. $^{222}Rn$ measurements

$^{222}Rn$ activities in water were measured in the Middle Paraná River near the western and eastern banks of each studied cross-section. Measures were also performed at the Upper Paraná and Paraguay rivers, as well as in groundwater samples. Measurements were carried out in situ using a RAD-7 equipment (Durridge Co.), a portable continuous radon-in-air monitor modified for radon-in-water that determines the activity of $^{222}Rn$ by counting its alpha-emitting daughters ($^{218}Po$ and/or $^{214}Po$). The RAD-7 uses a high electric field with a silicon semiconductor

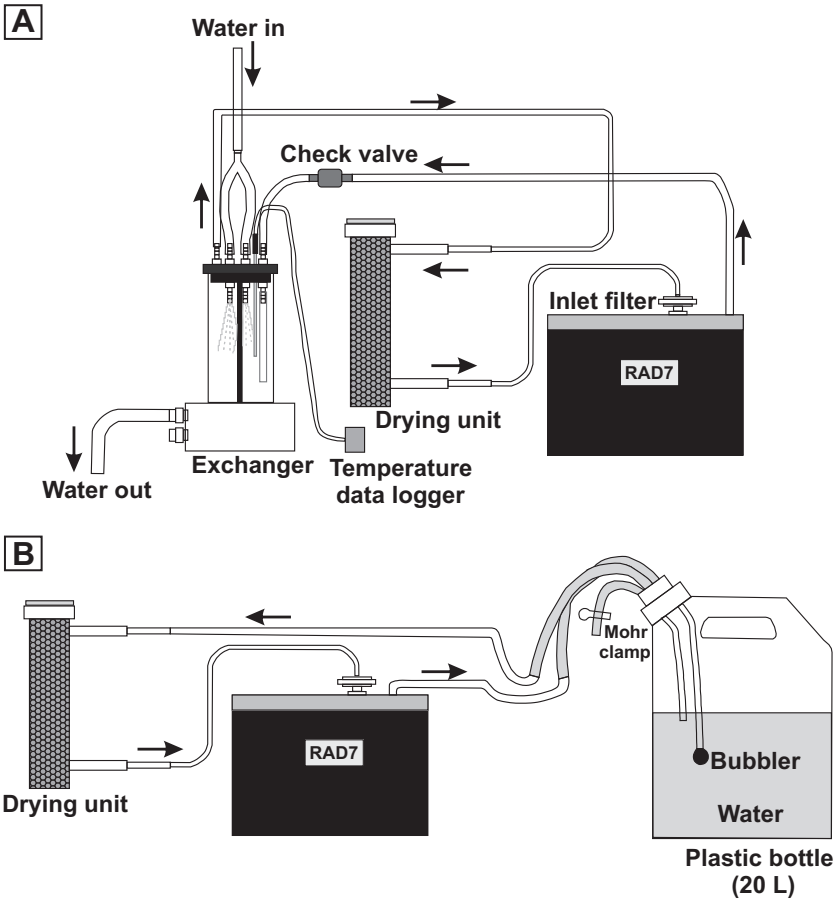


**Fig. 4.** Sampling setup for measuring $^{222}Rn$ in: (A) surface water; and (B) groundwater.

detector at ground potential to attract the positively-charged polonium daughters.

$^{222}$Rn activity in surface waters was measured using an air–water exchanger, a plastic cylinder where radon outgasses from water until solubility equilibrium is reached (Fig. 4A). The air is circulated in a closed loop and the exchanger is connected to the alpha radon detector via a drying unit which removes the water vapor. Groundwater samples were collected in 20 L plastic bottles designed to avoid gas loss (Stringer and Burnett, 2004) and $^{222}$Rn activity was measured in field using the RAD-7 (Fig. 4B). The sample bottle is connected to the RAD-7 via a closed air loop, and the internal pump of the detector re-circulates the air purging radon in water in order to achieve a rapid equilibrium of radon between water and air. The duration of each time series for ground- and surface waters was of 80 min and a new radon concentration was obtained every 20 min. The accuracy of the instrument is within

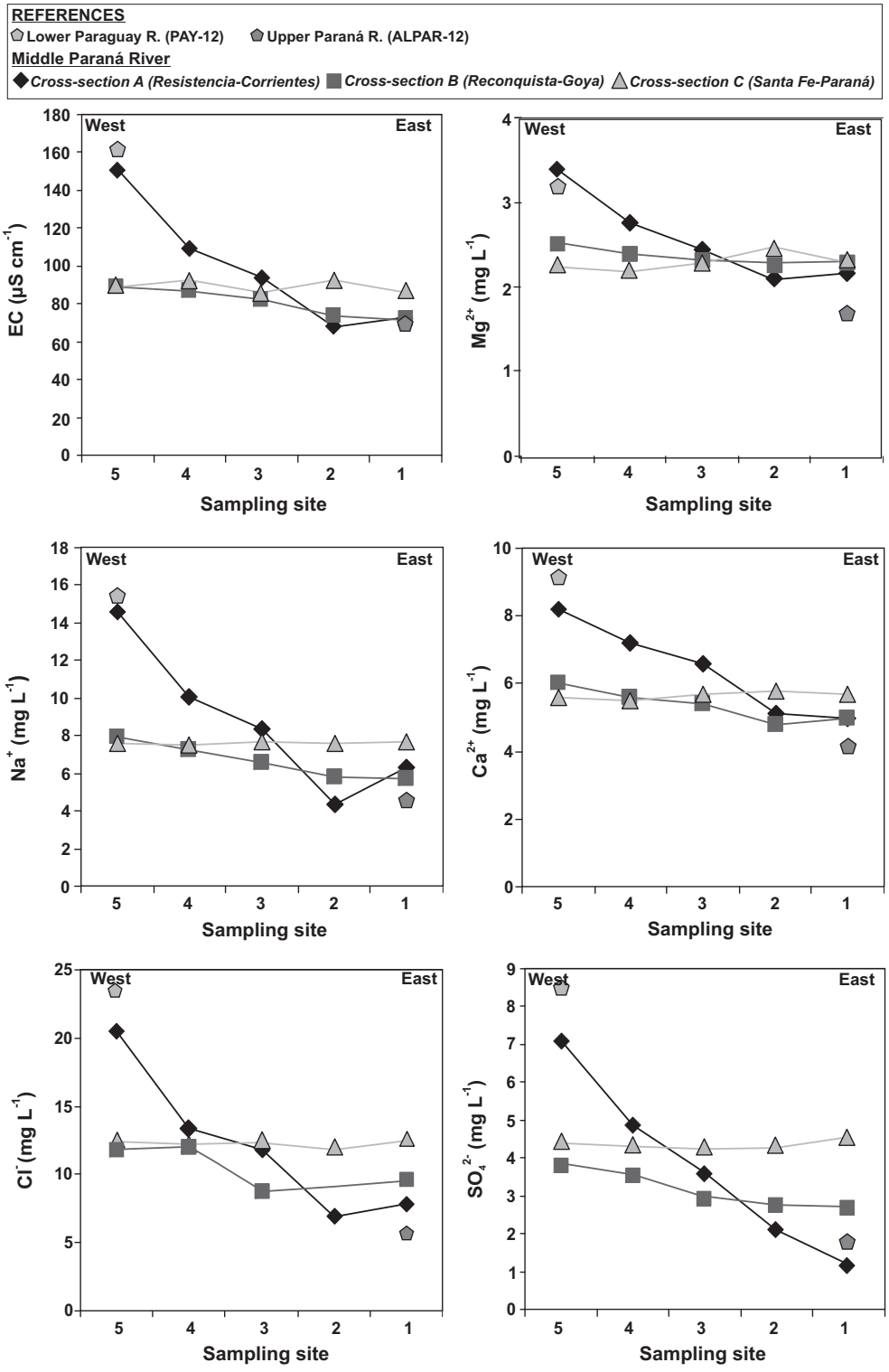


**Fig. 5.** Transverse variability of EC and major ions in the studied cross-sections. Corresponding values measured in the Paraguay and Upper Paraná rivers are also shown.

4% and its typical relative precision is <3% at 10,000 Bq $m^{-3}$, increasing to ~10% at 100 Bq $m^{-3}$. As the $^{222}$Rn partitioning between gas and liquid phases is controlled by temperature, the solubility coefficients were determined by continuous temperature measurements (Burnett et al., 2001), performed every 5 min using a HOBO data logger (Onset Co). When using the plastic bottle, temperature was measured with a conductivity/TDS meter (Hach Co) at the begging and at the end of each $^{222}$Rn determination.

## 4. Results

### 4.1. The major ion composition

Table 1 shows the physico-chemical parameters, the concentration of major ions and selected trace elements, and the stable isotope composition determined in surface and ground-water samples.

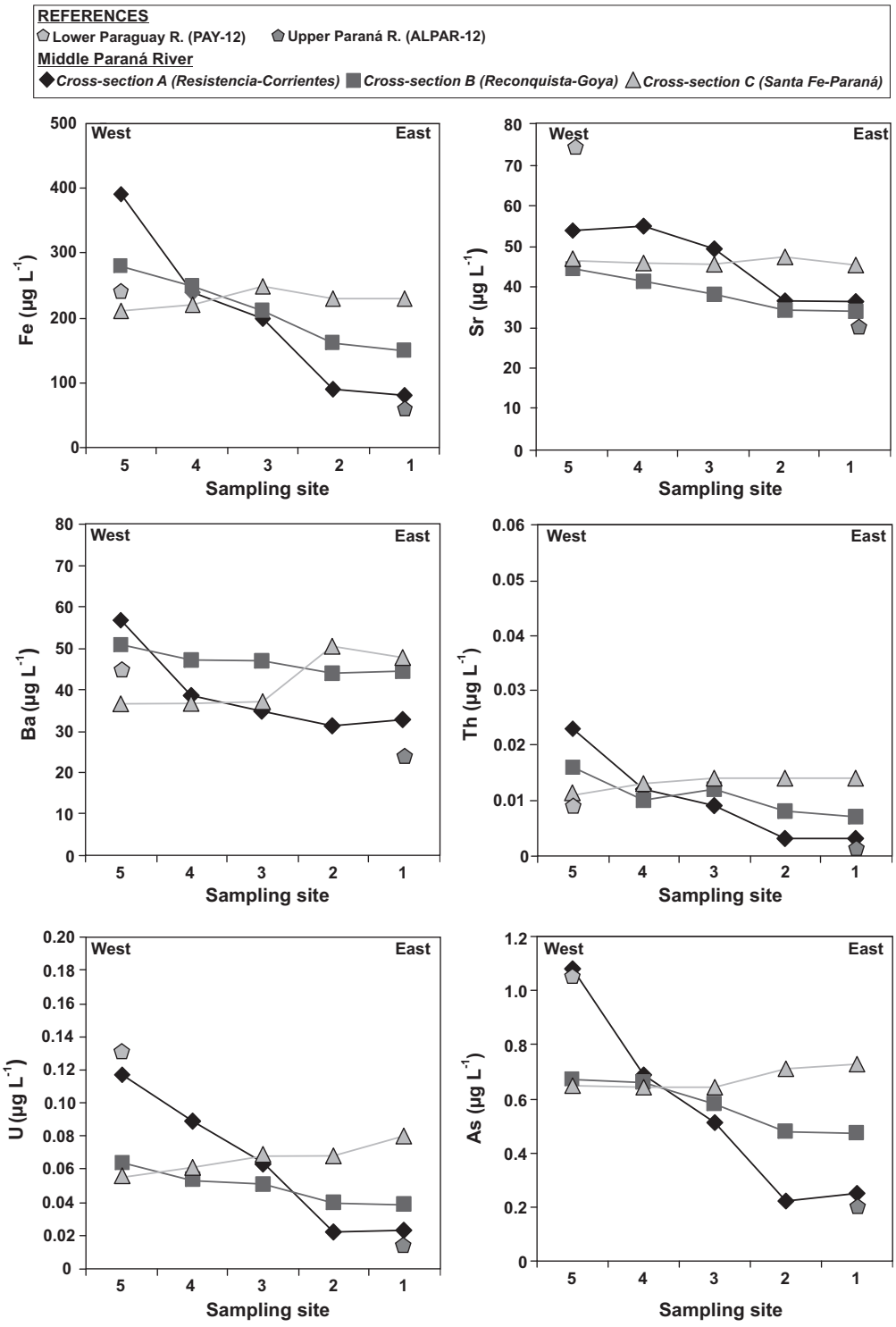


**Fig. 6.** Transverse variability of trace elements in the studied sampling cross-sections. Corresponding values measured in the Paraguay and Upper Paraná rivers are also shown.

**Table 2**
Dissolved rare earth elements (REE) concentrations, ∑REE, Eu and Ce anomalies, and $La_N/Yb_N$ ratios in the Middle Paraná River, its tributaries and aquifers. The Eu and Ce anomalies were calculated as follows: $(Eu/Eu^*)_N = Eu/(Sm^*Gd)^{0.5}$ and $(Ce/Ce^*)_N = Ce/(1/3Nd + 2/3La)$.

| River/aquifer | Sample no. | La | Ce | Pr | Nd | Sm | Eu | Gd | Tb | Dy | Ho | Er | Tm | Yb | Lu | ∑ETR | $(Eu/Eu^*)_N$ | $(Ce/Ce^*)_N$ | $La_N/Yb_N$ |
|---|---|---|---|---|---|---|---|---|---|---|---|---|---|---|---|---|---|---|---|
| | | $\mu g\ L^{-1}$ | | | | | | | | | | | | | | | | | |
| Middle Paraná R. | PARC2-11 | 0.146 | 0.273 | 0.026 | 0.099 | 0.024 | 0.009 | 0.024 | 0.003 | 0.017 | 0.003 | 0.009 | 0.001 | 0.007 | 0.002 | 0.643 | 1.76 | 0.95 | 1.53 |
| Cross-section A | PARC2-21 | 0.109 | 0.220 | 0.026 | 0.101 | 0.029 | 0.007 | 0.022 | 0.003 | 0.016 | 0.003 | 0.010 | 0.001 | 0.008 | 0.001 | 0.556 | 1.30 | 0.92 | 1.00 |
| | PARC2-31 | 0.353 | 0.545 | 0.052 | 0.208 | 0.055 | 0.012 | 0.043 | 0.006 | 0.029 | 0.006 | 0.016 | 0.001 | 0.010 | 0.002 | 1.338 | 1.16 | 0.81 | 2.59 |
| | PARC2-41 | 0.231 | 0.459 | 0.060 | 0.241 | 0.064 | 0.016 | 0.051 | 0.008 | 0.037 | 0.007 | 0.017 | 0.002 | 0.014 | 0.002 | 1.209 | 1.32 | 0.87 | 1.21 |
| | PARC2-51 | 0.344 | 0.739 | 0.102 | 0.415 | 0.097 | 0.024 | 0.089 | 0.012 | 0.058 | 0.010 | 0.029 | 0.003 | 0.024 | 0.003 | 1.949 | 1.21 | 0.89 | 1.05 |
| Middle Paraná R. | PARG2-11 | 0.150 | 0.349 | 0.043 | 0.169 | 0.041 | 0.012 | 0.040 | 0.005 | 0.025 | 0.005 | 0.013 | 0.002 | 0.013 | 0.002 | 0.869 | 1.39 | 0.99 | 0.85 |
| Cross-section B | PARG2-21 | 0.156 | 0.354 | 0.046 | 0.191 | 0.047 | 0.013 | 0.042 | 0.006 | 0.027 | 0.005 | 0.015 | 0.002 | 0.013 | 0.002 | 0.919 | 1.37 | 0.94 | 0.88 |
| | PARG2-31 | 0.198 | 0.444 | 0.055 | 0.234 | 0.059 | 0.017 | 0.051 | 0.007 | 0.036 | 0.006 | 0.017 | 0.003 | 0.019 | 0.002 | 1.148 | 1.46 | 0.94 | 0.76 |
| | PARG2-41 | 0.207 | 0.465 | 0.059 | 0.241 | 0.062 | 0.017 | 0.053 | 0.008 | 0.038 | 0.007 | 0.018 | 0.002 | 0.018 | 0.003 | 1.198 | 1.39 | 0.94 | 0.84 |
| | PARG2-51 | 0.294 | 0.625 | 0.078 | 0.307 | 0.080 | 0.021 | 0.069 | 0.010 | 0.046 | 0.009 | 0.025 | 0.003 | 0.019 | 0.003 | 1.589 | 1.33 | 0.93 | 1.13 |
| Middle Paraná R. | PARP2-11 | 0.220 | 0.485 | 0.063 | 0.249 | 0.070 | 0.018 | 0.058 | 0.008 | 0.040 | 0.007 | 0.020 | 0.003 | 0.016 | 0.003 | 1.260 | 1.33 | 0.94 | 1.01 |
| Cross-section C | PARP2-21 | 0.216 | 0.486 | 0.063 | 0.261 | 0.067 | 0.015 | 0.054 | 0.009 | 0.043 | 0.008 | 0.020 | 0.002 | 0.017 | 0.002 | 1.263 | 1.17 | 0.93 | 0.93 |
| | PARP2-31 | 0.242 | 0.539 | 0.072 | 0.293 | 0.073 | 0.019 | 0.065 | 0.009 | 0.043 | 0.008 | 0.019 | 0.002 | 0.018 | 0.003 | 1.405 | 1.30 | 0.92 | 0.99 |
| | PARP2-41 | 0.250 | 0.496 | 0.061 | 0.243 | 0.064 | 0.017 | 0.061 | 0.008 | 0.038 | 0.007 | 0.019 | 0.002 | 0.019 | 0.003 | 1.288 | 1.28 | 0.89 | 0.96 |
| | PARP2-51 | 0.193 | 0.444 | 0.056 | 0.226 | 0.052 | 0.013 | 0.057 | 0.007 | 0.037 | 0.006 | 0.018 | 0.002 | 0.016 | 0.002 | 1.129 | 1.12 | 0.97 | 0.88 |
| Paraguay R. | PAY-12 | 0.218 | 0.473 | 0.063 | 0.267 | 0.067 | 0.019 | 0.058 | 0.009 | 0.041 | 0.008 | 0.022 | 0.003 | 0.020 | 0.003 | 1.271 | 1.43 | 0.89 | 0.80 |
| Upper Paraná R. | ALPAR-12 | 0.065 | 0.141 | 0.016 | 0.072 | 0.018 | 0.005 | 0.016 | 0.002 | 0.010 | 0.002 | 0.006 | <0.001 | 0.007 | <0.001 | 0.360 | 1.38 | 0.93 | 0.68 |
| Empedrado R. | R-EMP | 0.784 | 1.810 | 0.241 | 0.989 | 0.236 | 0.063 | 0.227 | 0.031 | 0.144 | 0.027 | 0.077 | 0.009 | 0.071 | 0.010 | 4.719 | 1.28 | 0.94 | 0.81 |
| Corrientes R. | R-CORR12 | 0.259 | 0.522 | 0.074 | 0.309 | 0.070 | 0.021 | 0.068 | 0.010 | 0.050 | 0.009 | 0.025 | 0.003 | 0.026 | 0.004 | 1.450 | 1.43 | 0.84 | 0.73 |
| Santa Lucía R. | R-SLU | 0.089 | 0.160 | 0.023 | 0.107 | 0.029 | 0.011 | 0.025 | 0.003 | 0.018 | 0.003 | 0.011 | 0.001 | 0.011 | 0.002 | 0.493 | 1.92 | 0.75 | 0.59 |
| Guayquiraró R. | R-GUAYQ | 0.561 | 1.140 | 0.152 | 0.637 | 0.167 | 0.038 | 0.146 | 0.021 | 0.101 | 0.021 | 0.056 | 0.007 | 0.054 | 0.008 | 3.109 | 1.14 | 0.86 | 0.76 |
| Salado R. | ASAL-CH | 1.240 | 2.670 | 0.352 | 1.430 | 0.361 | 0.075 | 0.309 | 0.042 | 0.200 | 0.036 | 0.098 | 0.013 | 0.086 | 0.012 | 6.924 | 1.06 | 0.91 | 1.06 |
| Negro R. | R-NEG | 0.048 | 0.078 | 0.008 | 0.042 | 0.013 | 0.014 | 0.013 | 0.002 | 0.009 | 0.003 | 0.007 | <0.001 | 0.009 | 0.005 | 0.251 | 5.06 | 0.76 | 0.39 |
| Tapenagá R. | A-TAP | 0.857 | 1.860 | 0.228 | 0.972 | 0.267 | 0.058 | 0.250 | 0.034 | 0.166 | 0.031 | 0.087 | 0.011 | 0.075 | 0.012 | 4.908 | 1.05 | 0.92 | 0.84 |
| El Rey R. | A-REY | 1.890 | 4.630 | 0.556 | 2.240 | 0.580 | 0.122 | 0.508 | 0.072 | 0.349 | 0.061 | 0.166 | 0.021 | 0.157 | 0.024 | 11.376 | 1.06 | 1.02 | 0.88 |
| Toropí–Yupoí Aq. | POPAR-GOY1 | 0.029 | 0.055 | 0.006 | 0.025 | 0.006 | 0.010 | 0.007 | <0.001 | 0.005 | <0.001 | 0.003 | <0.001 | 0.003 | <0.001 | 0.149 | 7.25 | 0.89 | 0.71 |
| Transition to | POPAR-REC1 | 0.012 | 0.023 | 0.001 | 0.006 | 0.001 | <0.001 | 0.003 | <0.001 | <0.001 | 0.001 | 0.002 | <0.001 | <0.001 | <0.001 | 0.049 | | | |
| Puelches Aq. | POPAR-REC2 | 0.027 | 0.035 | 0.003 | 0.009 | 0.003 | 0.025 | 0.007 | <0.001 | 0.002 | <0.001 | 0.001 | <0.001 | 0.002 | <0.001 | 0.114 | 25.64 | 0.76 | 0.99 |
| Ituzaingó Aq. | POPAR-CORR | 0.024 | 0.035 | 0.002 | 0.008 | 0.003 | 0.003 | 0.003 | <0.001 | 0.001 | <0.001 | <0.001 | <0.001 | <0.001 | <0.001 | 0.079 | 4.70 | 0.86 | |
| | POPAR-GOY2 | 0.028 | 0.038 | 0.002 | 0.011 | 0.003 | 0.008 | 0.003 | <0.001 | <0.001 | <0.001 | <0.001 | <0.001 | 0.002 | <0.001 | 0.095 | 12.53 | 0.78 | 1.03 |
| Paraná Aq. | POPARg-12 | 0.009 | 0.018 | 0.003 | 0.011 | 0.004 | 0.002 | 0.002 | <0.001 | 0.002 | <0.001 | <0.001 | <0.001 | 0.001 | <0.001 | 0.052 | 3.32 | 0.82 | 0.66 |

To characterize the chemical transverse variability in the main channel of the Middle Paraná River, only data corresponding to samples taken at ~15 cm were considered, as no vertical inhomogeneities were found along the water column in the analyzed cross-sections. Neutral to slightly alkaline conditions prevailed all along the analyzed stretch, with pH values that ranged between 7.02 and 7.39. Eh values ranged between 352 and 418 mV, indicating that postoxic conditions predominate even though dissolved oxygen is present likely as a consequence of redox disequilibrium. Neither transverse nor longitudinal variations were recognized in pH and Eh values. Unlike these parameters, a marked variation was observed in EC values, which ranged between 67.8 and 150.5 μS cm$^{-1}$ from the eastern to the western bank in cross-section A (Table 1, Fig. 5). This variability was less evident at cross-section B, where the EC registered in the western margin was 1.25 times higher than in the eastern border and completely disappeared at cross-section C (Table 1). Measured TDS values (mean 45 mg L$^{-1}$) were in the range of some other world large rivers such as the Amazon (~44 mg L$^{-1}$) and Congo (~35 mg L$^{-1}$) (e.g., Gaillardet et al., 1999).

The main tributaries (i.e., Paraguay and Upper Paraná rivers) were slightly acidic to slightly alkaline, with pH values that ranged between 6.8 and 7.8 (Table 1). The Paraguay River registered an EC value of 162 μS cm$^{-1}$, which resulted 2.4 times higher than the one measured in the Upper Paraná River (68.7 μS cm$^{-1}$). Waters reaching the main channel from minor eastern tributaries downstream the confluence of Paraguay and Upper Paraná rivers (i.e., Empedrado, Corrientes, Santa Lucía and Guayquiraró rivers) were slightly dilute (242 < EC < 436 μS cm$^{-1}$), whereas western tributaries (i.e., Salado in Chaco province, Negro, Tapenagá and El Rey rivers) showed variable EC values (259 < EC < 2,920 μS cm$^{-1}$), from slightly dilute to slightly saline (Table 1).

The relative concentration of major cations at the three cross-sections of the Middle Paraná River was $Na^+ > Ca^{2+} > Mg^{2+} > K^+$, keeping the trend measured in the Upper Paraná and Paraguay rivers. $Na^+$ and $HCO_3^-$ were the most abundant ions in the analyzed river stretch, accounting for ~40% and ~60% of the total concentration of major cations and anions respectively.

According to their anionic composition, waters at cross-section A evolved from $HCO_3^-$ type in the eastern margin, to $Cl^-$ type in the West. At cross-sections B and C, a slight evolution from $HCO_3^-Cl^-$–$SO_4^{2-}$ type to $HCO_3^-$ type was observed from East to West. The cationic composition was less variable than the anionic one, as the waters were of the $Na^+$–$Ca^{2+}$ type at the three cross-sections.

Major species $Ca^{2+}$, $Na^+$, $Mg^{2+}$, $Cl^-$ and $SO_4^{2-}$ also showed a transverse asymmetry at the middle stretch (Table 1, Fig. 5), consistent with the observations of Drago and Vasallo (1980). As well as for EC, a trend of increasing concentrations was observed from East to West at cross-sections A and B, while at the downstream cross-section C, the trend was just opposite (Fig. 5). At cross-section A, $Na^+$ was 2.3 times higher in the western margin than in the eastern one, whereas $Ca^{2+}$ and $Mg^+$ were 1.6 times higher. Major anions $Cl^-$ and $SO_4^{2-}$ were 2.6 and 5.9 times higher respectively, in the western border of cross-section A compared to the eastern margin. This chemical asymmetry was less pronounced at cross-section B.

The major chemical composition determined in the two main tributaries, Upper Paraná and Paraguay rivers, was dominated by waters of the $Na^+$–$Ca^{2+}$–$HCO_3^-$ and $Na^+$–$HCO_3^-$–$Cl^-$–$SO_4^{2-}$, respectively. Water in minor eastern tributaries were of the $Na^+$–$Cl^-$ type, while water in minor western tributaries showed a chemical composition dominated by $Na^+$–$HCO_3^-$–$Cl^-$–$SO_4^{2-}$ type.

Groundwater samples were acid to slightly alkaline, with pH values ranging from 5.91 to 7.14 (Table 1). EC ranged between 194 and 1,830 μS cm$^{-1}$. The lower EC values (~194 μS cm$^{-1}$) were measured at the Ituzaingó Aquifer (samples POPAR-CORR and POPAR-GOY2), followed by the Toropí–Yupoí Aquifer (sample POPAR-GOY1), with an EC value of ~370 μS cm$^{-1}$. Higher EC values (~856 μS cm$^{-1}$) were determined at Transition to Puelches Aquifer (samples POPAR-REC1 and POPAR-REC2), whereas at the Paraná Aquifer (sample POPARg-12) an EC value two times higher (~1,830 μS cm$^{-1}$) was detected (Table 1). According to their major chemical composition, groundwater varied from the $HCO_3^-$ type to the $Cl^-$ type and they were of the $Na^+$-type or of the $Na^+$–$Ca^{2+}$ type in terms of cationic composition.

### 4.2. Trace elements

Trace elements also showed a transverse variability in the Middle Paraná stretch, that was more evident regarding the concentrations of Fe, U, Th, Ba, Sr and As (Table 1, Fig. 6). At cross-sections A and B increasing concentrations of these trace

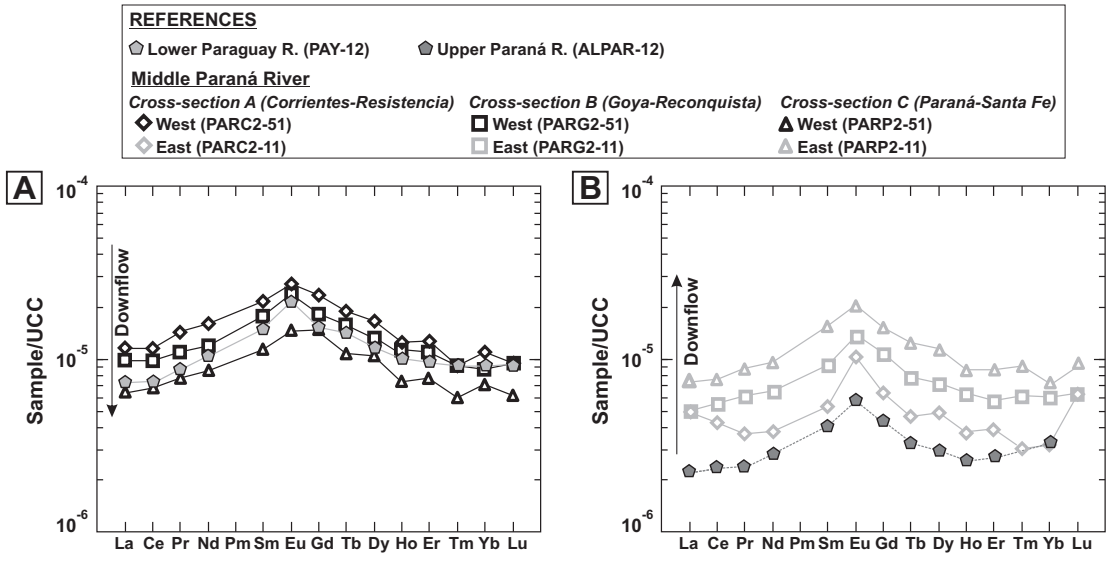


**Fig. 7.** UCC-normalized REE spidergrams for the samples of the Middle Paraná River and main tributaries. (A) Samples collected from the western margin and Paraguay River. (B) Samples collected from the eastern border and Upper Paraná River.

elements were observed from East to West, whereas at cross-section C, an opposite trend was distinguished.

Dissolved rare earth elements (REE) concentrations and some calculated REE relationships in water samples of the Paraná basin are shown in Table 2. REE trends have been particularly analyzed here because they are good tracers of sediment and solute provenance (e.g., Aubert et al., 2001; García et al., 2007; Sholkovitz et al., 1999; Tweed et al., 2006). The total dissolved REE concentration in the Middle Paraná River ranged from ~550 ng $L^{-1}$ to ~1,590 ng $L^{-1}$, with a mean concentration of 1,184 ng $L^{-1}$. Compared to other tropical basins, the mean REE concentration is slightly higher than the one measured in the Amazon (mean ~990 ng $L^{-1}$) and lower than the one registered at the Congo basin (mean ~1860 ng $L^{-1}$) (e.g., Dupré et al., 1996; Gaillardet et al., 1997). Following the trend described for major and trace elements, the REEs also showed a transverse variability along the sampling cross-sections, i.e., increasing concentrations from East to West were observed in cross-sections A and B, while at cross-section C a less pronounced and opposite trend was observed. Besides, in the Upper Paraná River the measured REE concentrations were lower than in the Lower Paraguay River.

For the present analysis, the concentrations of REE measured in the western and eastern margins of the studied stretch were normalized to the corresponding values in the Upper Continental Crust (UCC, McLennan, 2001), and the obtained spider diagrams are shown in Fig. 7A and B respectively. In general, all samples showed similar patterns, characterized by a pronounced convexity in the middle REEs (MREE, Sm, Eu and Gd). The MREE-enriched UCC-normalized pattern displayed by the Middle Paraná River along the three cross-sections, has been identified in many rivers and it was attributed to the weathering of MREE-enriched Fe–Mn oxyhydroxides (Fernández-Caliani et al., 2009; Johannesson and Zhou, 1999), the weathering of MREE-enriched phosphate minerals (Hannigan and Sholkovitz, 2001), the presence of MREE-enriched colloidal material (e.g., Elderfield et al., 1990; Ingri et al., 2000; Sholkovitz, 1995), or enhanced complexation of the MREEs with dissolved organic matter (Johannesson et al., 2004).

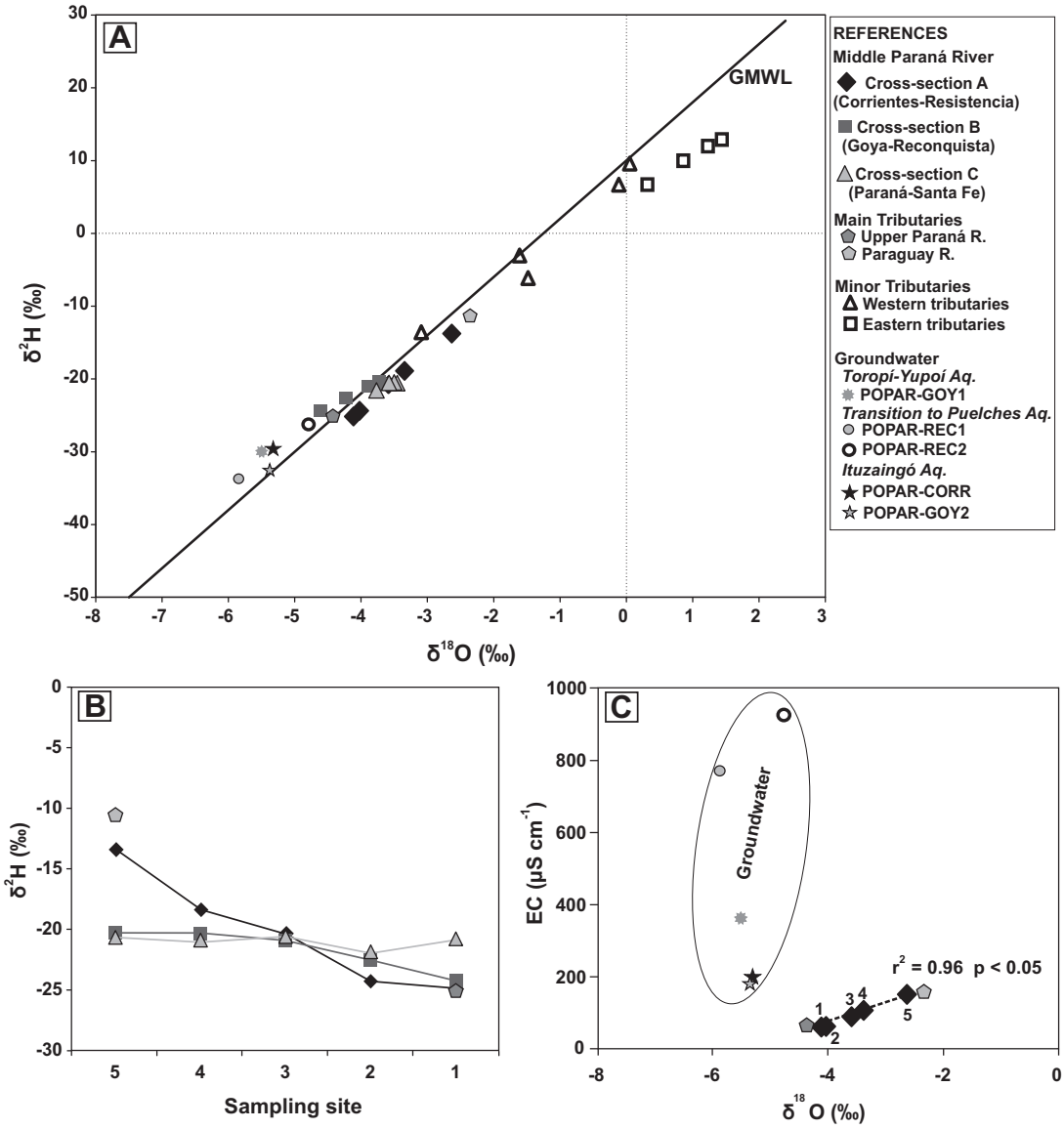


**Fig. 8.** (A) $\delta^2H$ vs $\delta^{18}O$ plot showing the isotopic signature of surface water samples from the Middle Paraná River, tributaries and groundwater. Solid line denotes the Global Meteoric Water Line (GWML). (B) Transverse variability of $\delta^2H$ at the sampled cross-sections. The corresponding isotopic values of the Paraguay and Upper Paraná rivers are plotted for comparison. (C) Plot showing the EC vs. $\delta^{18}O$ in water from cross-section A. The end-members correspond to the Paraguay and Upper Paraná rivers.

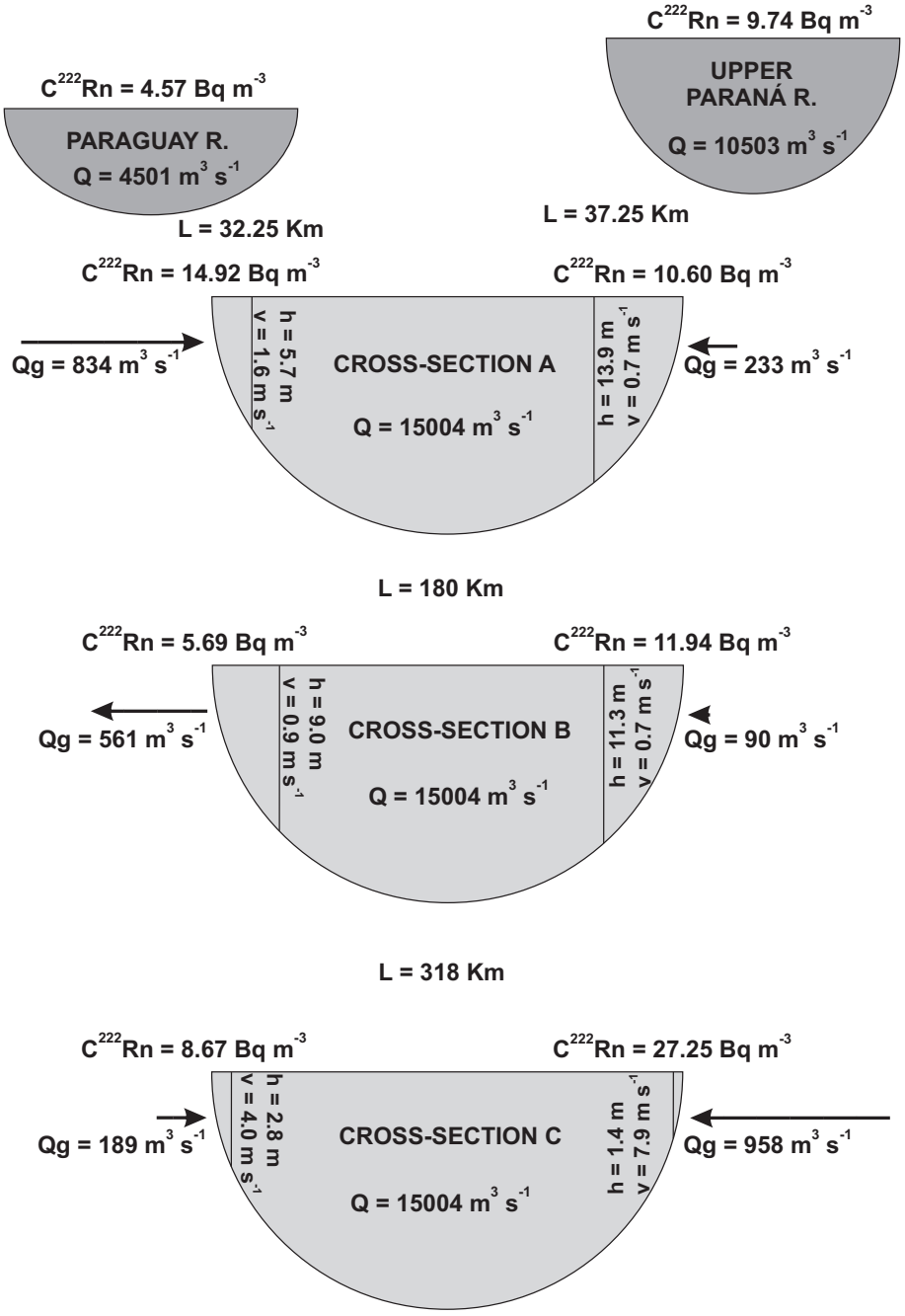


**Fig. 9.** Mass-balance model calculated from $^{222}$Rn activities showing the water contributions to the Middle Paraná River from different hydrological compartments. The parameters used for calculation are also indicated.

Before their confluence, the Paraguay and Upper Paraná rivers both exhibited HREE-enriched UCC-normalized concentrations ($La_N/Yb_N$ = 0.80 and 0.68, respectively), the absolute concentrations being about one order of magnitude higher in the first river (Table 2). After the confluence, slightly LREE-enriched UCC-normalized patterns predominated all along cross-section A ($La_N/Yb_N$ ratios ranging from 1.00 to 2.59), and higher fractionation was observed in the eastern margin. Because the absolute concentration of HREEs measured in the eastern and western margins at cross-section A were similar to those measured in the Upper Paraná and Paraguay rivers respectively (Table 2), the above mentioned change must be assigned to increasing concentration of LREEs in this section. Depetris and Pasquini (2007) reported the average REE values measured in suspended sediments collected from the Middle Paraná. These values were normalized to the UCC, and the obtained spidergrams resulted typically LREE enriched, which suggests that dissolution of REE-bearing minerals present in these sediments and/or the preferential detachment of LREEs from adequate surfaces could be responsible for the observed increase in LREE concentrations. Downflow, in cross-sections B and C, the fractioning between LREEs and HREEs is almost negligible ($La_N/Yb_N$ ratios ranging from 0.76 to 1.13; Fig. 7B, Table 2). One interesting feature observed in Fig. 7 is that in the western margin, the concentration of REEs decreased downflow, while in the East, the opposite trend was observed.

Positive Eu anomalies were calculated in all samples (Table 2). The samples from the middle stretch showed similar $(Eu/Eu^*)_N$ ratios (average value 1.33) than the Paraguay and Upper Paraná

rivers (1.43 and 1.38, respectively). In general, samples collected from the eastern margin showed higher $(Eu/Eu^*)_N$ ratios than in the West, and the same was determined for all the minor eastern tributaries. Positive $(Eu/Eu^*)_N$ in surface waters are generally attributed to the preferential weathering of plagioclase, which are usually Eu-enriched due to the substitution of $Sr^{2+}$ with $Eu^{2+}$ in Ca-plagioclase (e.g., McLennan, 1989).

Groundwater samples exhibited lower total dissolved REE concentrations compared to surface waters (from ~50 ng $L^{-1}$ to ~150 ng $L^{-1}$). Their UCC-normalized concentrations (not shown) are enriched in HREEs, with the exception of water collected from the Ituzaingó Aquifer which was slightly enriched in LREEs. Strong positive Eu anomalies were calculated for all the analyzed groundwater samples (Table 2).

### 4.3. Trends in stable isotopes

The stable isotopic composition of samples collected in November 2012 in the studied stretch of the Paraná River is shown in Table 1. The values of $\delta^{18}O$ measured in the studied river sections varied between −4.6‰ and −2.7‰, while $\delta^2H$ ranged between −25‰ and −13‰. Panarello and Dapeña (2009) measured similar $\delta^{18}O$ and $\delta^2H$ ratios (between −4.2‰ and −3.3‰ for $\delta^{18}O$ and between −30‰ and −15‰ for $\delta^2H$) for November in the period encompassed between 1997 and 2006 at the Río de la Plata estuary, ~435 km downflow cross-section C. Fig. 8 shows the isotopic signature of the surface and ground-water samples analyzed in this study. All surface waters collected along the three cross-sections plot over the Global Meteoric Water Line (GMWL), defined as $\delta^2H = 8\delta^{18}O + 10$ (Craig, 1961), suggesting that evaporation in the main channel was almost negligible. The isotopic signature of water along the analyzed stretch was nearly the same and resulted more fractionated than waters flowing from the minor tributaries that reach the main channel from the western and eastern banks. Minor tributaries from the eastern margin plot below the GMWL, suggesting that they were affected in some extent by evaporation.

Pasquini and Depetris (2010) established that the $\delta^{18}O$ signature of the Middle Paraná River water seems to be considerably tied to the relative contribution of each individual headwater, i.e., the Upper Paraná and the Paraguay drainage basins. Concordantly, the isotopic signature of water in the three cross-sections studied here was just intermediate between those of the main tributaries. This clearly reveals the mixing of waters and indicates that neither some other sources nor evaporation have affected the observed isotopic signature. As a general trend, water flowing on the western margin was less fractionated (i.e., more enriched in heavy isotopes) and showed the same isotopic signature as the Paraguay River, while water on the eastern margin was more fractionated and exhibited an isotopic signature that resembled that of the Upper Paraná River (Fig. 8B). As expected, this trend is more noticeable in the upstream cross-section A, while at cross-section C, all samples showed similar isotopic signature, indicating a complete mixing.

The isotopic signature of groundwater samples suggested a common recharge from meteoric waters for all the aquifers, but the source seems to be independent of the surface water contributions, as they were all more fractionated than surface waters (Fig. 8A).

## 5. Factors that trigger the transverse chemical variability in the Middle Paraná River

As observed in many other parts of the world, the confluence of two large rivers triggers transverse and vertical inhomogeneities in the dissolved and particulate fractions that may extend for several kilometers. The characterization of this variability may help to define the extent of the mixing process, as well as to define the transport and mobility of solutes in the flow direction.

The Upper Paraná and Paraguay rivers show different chemical signatures that reflect the geochemical environment of their respective drainage basins. The Paraguay basin is covered primarily by Neogene and recent fluvial deposits. Outcrops of the Cretaceous basalts of the Brazilian Paraná basin occur in its northeastern portion (e.g., Milani and Zalán, 1999). The Bermejo and Pilcomayo rivers discharge in the lower reach of the Paraguay River. In its headwaters, at the Andes foothills, a number of rock types can be found where lutites, phyllites and fine-grained sediments predominate (Iriondo and Praira, 2007). They are responsible for the high load of sediments observed in the Middle Paraná River, as the Pilcomayo River carries about $9.8 \times 10^7$ t $yr^{-1}$ of sediments (Facetti-Masulli and Klump, 2010) and the Bermejo River delivers more than $1 \times 10^8$ t $yr^{-1}$of sediments, of which 98% corresponds to the suspended load (Orfeo and Iriondo, 2012). On the other hand, the Cretaceous tholeiitic basalts of the Serra Geral Formation and the continental sands and sandstones of the Baurú Group (Upper Cretaceous) predominate in the Upper Paraná basin. Precambrian metamorphic rocks are also found in its headwaters. The dominance of crystalline rocks in the Upper Paraná basin results in a much lower load of both, suspended and dissolved matter, compared with the inputs from the Paraguay River. Thus, the Paraguay River shows solute contents that result 2–5 times more concentrated than waters in the

**Table 3**
$^{222}Rn$ activities measured on surface and groundwater samples, parameters used in the mass-balance calculation and calculated groundwater discharge at the river banks of the Middle Paraná River. River discharge data was obtained from Argentina's Subsecretaría de Recursos Hídricos (www.hidricosargentina.gov.ar).

| River/aquifer | Sampling site | $C^{222}Rn$ (Bq $m^{-3}$) | $Q$ ($m^3$ $s^{-1}$) | $h$ (m) | $v$ (m $s^{-1}$) | $L$ (km) | $Q_g$ ($m^3$ $s^{-1}$) Transition to Puelches | Ituzaingó | Paraná |
|---|---|---|---|---|---|---|---|---|---|
| Paraguay R. | Middle of the channel | 4.57 | 4501 | 2.5 | 4.8 | | | | |
| Upper Paraná R. | Middle of the channel | 9.74 | 10,503 | 10.3 | 0.4 | | | | |
| Middle Paraná R. Section A | East | 10.60 | 15,004 | 13.9 | 0.7 | 37.25 | 67 | 142 | 24 |
| | West | 14.92 | 15,004 | 5.7 | 1.6 | 32.25 | 241 | 507 | 86 |
| Middle Paraná R. Section B | East | 11.94 | 15,004 | 11.3 | 0.7 | 180 | 26 | 55 | 9 |
| | West | 5.69 | 15,004 | 9 | 0.9 | 180 | −162 | −341 | −58 |
| Middle Paraná R. Section C | East | 27.25 | 15,004 | 1.4 | 7.9 | 318 | 277 | 583 | 98 |
| | West | 8.67 | 15,004 | 2.8 | 4.0 | 318 | 55 | 115 | 19 |
| Transition to Puelches Aq. | POPAR-REC2 | 844.80 | | | | | | | |
| Ituzaingó Aq. | POPAR-CORR | 137.50 | | | | | | | |
| | POPAR-GOY2 | 664.60 | | | | | | | |
| Paraná Aq. | POPARg-12 | 2376.48 | | | | | | | |

Upper Paraná River. Besides, the isotopic signature has revealed clear differences between these two waters, as in the Paraguay River water stable isotopes are less fractionated and exhibit slight signals of evaporation.

Downstream the confluence, lateral chemical inhomogeneities have been detected whereas the chemical composition of water is uniform in depth. The highest variability in the elemental concentrations has been measured in cross-section A, immediately after the confluence of the Upper Paraná and Paraguay rivers.

In order to identify the relative contributions from the two main tributaries at cross-section A under baseflow conditions, a mass balance was performed by using Eq. (2) and the concentrations of the conservative anion $Cl^-$ measured in the tributaries and after their confluence:

$$[Cl^-]_{mixture} = x[Cl^-]_{Pay} + (1-x)[Cl^-]_{UP} \quad (2)$$

where $x$ is the fraction of water delivered by the Paraguay River and $1-x$ is the fraction of water delivered by the Upper Paraná River. Samples PAY-12, ALPAR-12, PARC2-11, PARC2-31, and PARC2-51 were used in the mass balance model. As expected, the contribution of the Paraguay River in the western margin of the Middle Paraná River reaches ~83% of the total discharge in this cross-section, and it decreases toward the East, reaching ~12% of the total discharge in the eastern margin.

Coupling $\delta^{18}O$ and EC measurements gives useful information about sources of water and mixing proportions (Lambs, 2000). The general trend of increasing EC with enrichment in $\delta^{18}O$ observed for cross-section A also reveals the mixing process of the main tributaries, as samples from the middle stretch plot between the end-members (Fig. 8C). On the contrary, in groundwater samples, the increasing EC values are independent of the observed isotopic fractionation.

At cross-section C (~580 km downstream the confluence), the chemical signature of the Paraguay River almost disappeared and a slight opposite trend regarding trace elements and stable isotopes was observed. This trend switch could be the result of contributions from minor tributaries that reach the main channel from the eastern margin, and/or may also be triggered by higher groundwater discharges at the eastern bank.

A number of studies have examined surface–groundwater interactions in lakes (e.g., Dimova et al., 2013; Kluge et al., 2012), coastal zones (e.g., Burnett and Dulaiova, 2003) and small rivers (e.g., Cartwright et al., 2011; Mullinger et al., 2007; Smerdon et al., 2012). The most common approaches for measuring groundwater discharge into surface waters are: (1) calculating groundwater flow through the application of Darcy's law (McBride and Pfannkuch, 1975); (2) direct measurements with seepage meters (Lee, 1977); (3) stream gauging (e.g. Cey et al., 1998); (4) temperature measurements (e.g., Cook et al., 2003); and (5) by using geochemical tracers (e.g., Cook et al., 2003; Dimova et al., 2013; Santos et al., 2008). $^{222}Rn$, an inert gas ($t_{1/2}$ = 3.8 days) produced by the radioactive decay of $^{238}U$, is one of the most powerful tracers to estimate groundwater discharge, since its activities in surface waters are two to three orders of magnitude lower than in groundwater due to degassing to the atmosphere and radioactive decay.

The $^{222}Rn$ activities were measured on selected surface and groundwater samples in order to evaluate the groundwater discharge into the middle stretch of the Paraná River (Table 3). In general, surface waters of the Middle Paraná River showed low $^{222}Rn$ activities, which varied from 5.7 to 27.2 Bq m$^{-3}$. Although $^{222}Rn$ activities measured in the Upper Paraná and Paraguay rivers were in the same range of the middle stretch, the first one registered a $^{222}Rn$ activity two times higher than the one measured in the Paraguay River. At cross-section A, $^{222}Rn$ activities increased from East to West, whereas at cross-sections B and C a reverse trend was observed.

The $^{222}Rn$ activities in groundwater were 1–2 orders of magnitude higher than in surface water. Furthermore, they were highly variable depending on bedrock aquifer, as they ranged between 137.5 and 2376.5 Bq m$^{-3}$ (Table 3). Low radon values in groundwater are usually associated with low uranium contents in soil, conditions favoring radon emanation to the atmosphere, and/or very short residence times. In the study area, the lower $^{222}Rn$ activities were measured in the Ituzaingó Aquifer, composed of quarzitic sandstones, while in the Transition to Puelches Aquifer, the $^{222}Rn$ activities were two times higher. Highest activities were determined in groundwater collected from the deeper Paraná Aquifer.

Though more data is needed, the contribution from groundwater discharges into the Middle Paraná River was estimated, as a first approach, by solving a conceptual $^{222}Rn$ mass balance equation proposed by Hamada (1999):

$$Q_g = \frac{C_2Q_2 - C_1Q_1\ \exp(-aL)}{\frac{C_g(1-\exp(-aL))}{aL}} \quad (3)$$

where $Q_g$ is the groundwater inflow (m$^3$ s$^{-1}$), $C_1$ and $C_2$ are the $^{222}Rn$ concentrations in river water at the upstream and downstream stations (Bq m$^{-3}$), respectively, $Q_1$ and $Q_2$ are the discharge rates at the upstream and downstream stations (m$^3$ s$^{-1}$), $C_g$ is the $^{222}Rn$ concentration in groundwater (Bq m$^{-3}$), and $L$ is distance between stations (km). $a$ is a parameter that can be calculated using Eq. (4).

$$a = (D/zh\upsilon) + (\lambda/\upsilon) \quad (4)$$

where $D$ is the molecular diffusivity of $^{222}Rn$,which in turn has been described by Peng et al. (1974) as a function of temperature $D = 10^{-(980/(T+273)+1.59)}$ ($1 \times 10^{-5}$ m$^2$ s$^{-1}$ at 25 °C); $z$ is the thickness of a stagnant film (m), which is about 20 μm when distance between stations is several kilometers (Hamada et al., 1997); $h$ is the average stream depth (m); $\upsilon$ is the average stream velocity (m s$^{-1}$); and $\lambda$ is the $^{222}Rn$ decay constant ($2.08 \times 10^{-6}$ s$^{-1}$).

Three groundwater end-members were established depending on the bedrock aquifer. A $^{222}Rn$ concentration of 845 Bq m$^{-3}$ was assigned to the Transition to Puelches Aquifer, while $^{222}Rn$ concentrations of 401 and 2376.5 Bq m$^{-3}$ were estimated for the Ituzaingó and Paraná Formations, respectively. For modeling purposes, the discharge in the Middle Paraná River has been considered constant in the studied stretch. The values of the parameters used in the mass-balance calculation are listed in Table 3, as well as the calculated groundwater discharge. Fig. 9 shows a schematic representation of the model and the obtained results. By comparing the estimated groundwater inflow with the November 2012 average discharge in the Middle Paraná River, it can be seen that groundwater contributed less than ~6% of the total water inputs all along the studied stretch. At cross-section A the groundwater discharge was greater in the western margin (~5.5% against ~1.5% in the East), whereas at cross-section C a reverse trend was observed, with contributions of ~6% in the East and ~1% in the West (Fig. 9). At cross-section B the modeled groundwater discharge in the western margin was negative (~−3.5%), which suggests the occurrence of river discharges into perched aquifers developed at the riveŕs bank. In the opposite margin, the groundwater inflow to the middle stretch was almost negligible (~0.5%).

## 6. Conclusions

In this study new chemical and stable and radiogenic isotopic data for the Paraná River drainage basin is presented in order to explain the dissimilar composition of water observed across the main channel of the Middle Paraná. After the confluence of the

Upper Paraná and Paraguay rivers the chemical asymmetry earlier observed by Drago and Vassallo (1980) was confirmed. It is mainly manifested through the values of EC, major ions ($Ca^{2+}$, $Na^{+}$, $Mg^{2+}$, $Cl^{-}$ and $SO_4^{2-}$), some trace elements (Fe, U, Th, Ba, Sr, As and REE), and particularly through the stable isotope composition ($\delta^{18}O$ and $\delta^{2}H$). This variability remained detectable downflow, until the cities of Reconquista and Goya (~225 km downflow the confluence).

Immediately after the confluence, the unmixing of waters is clear: in the sampling station located near the western margin at cross-section A, the major ion concentrations, the EC values and the stable isotope signature, were just slightly more diluted than the corresponding parameters measured in the Paraguay River, but higher than the corresponding values determined in the eastern border. There, on the contrary, waters preserved the chemical signature of the Upper Paraná River, showing just slightly higher concentrations.

The higher solute concentrations measured along the western bank of the Middle Paraná River at cross-section A, reflect the influence of the high load of suspended sediments supplied by the Paraguay River, which mostly originates at the Andes foothills and is transported downflow by the Bermejo River (e.g., Drago and Amsler, 1988; Amsler and Drago, 2009). The isotopic signature at cross-section A also reveals the mixing of the main tributaries, and according to mass-balance calculations based on $Cl^{-}$ concentrations it has been estimated that more than 80% of water in the western margin is supplied by the Paraguay River, whereas at the East, the contribution from this tributary is minor, as it accounts for less than 15% of the water budget in this cross-section.

About 225 km downflow the confluence, the cross-sectional chemical asymmetry was still observed, but differences between western and eastern margins were less evident. A slight inversion in the transverse chemical asymmetry was distinguished at about 580 km downflow the confluence. This trend switch can be assigned to the input of solutes from minor tributaries that reach the main channel from the eastern margin, as well as from groundwater inflow. Calculations using $^{222}Rn$ mass-balance indicate that groundwater inputs may account for about 0.5–6% of the total water inputs to the Middle Paraná River under baseflow conditions. These contributions are considered to be negligible in the chemical asymmetry observed after the confluence of the Paraguay and Upper Paraná rivers, but may partially explain the higher concentrations of some trace elements (i.e., As, Fe, U, Ba and Sr) measured in the eastern margin of the Middle Paraná River ~580 km downflow the confluence.

## Acknowledgements

Authors wish to acknowledge the assistance of Consejo Nacional de Investigaciones Científicas y Técnicas (CONICET, Argentina, PIP 112-200801-03160), Universidad Nacional de Córdoba, and the Agencia Nacional de Promoción Científica y Tecnológica (ANPCyT, PICT-2012-0275), which supported facilities used in this investigation. We also wish to acknowledge O. Orfeo and the staff of the Centro de Ecología Aplicada del Litoral (CECOAL – CONICET), K. Lecomte, and S. Formica for their assistance during the sampling campaign. Many thanks to S. Formica for the chromatographic determination of anions. We also thank P. Depetris for his constructive comments. V.A. Campodonico acknowledges a doctoral fellowship from CONICET. M.G. García and A.I. Pasquini are members of CICyT, CONICET. We are especially grateful to O. Sracek, one anonymous reviewer, and the Associate Editor P. Bhattacharya, for suggesting significant improvements to this manuscript.

## References

Amsler, M.L., Drago, E.C., 2009. A review of the suspended sediment budget at the confluence of the Paraná and Paraguay Rivers. Hydrol. Process. 23, 3230–3235.
Araujo, L., França, A.B., Potter, P., 1999. Hydrogeology of the Mercosul aquifer system in the Paraná and Chaco – Paraná Basins, South America, and comparison with the Navajo – Nugget aquifer system, USA. Hydrogeol. J. 7, 317–336.
Aubert, D., Stille, P., Probst, A., 2001. REE fractionation during granite weathering and removal by waters and suspended loads: Sr and Nd isotopic evidence. Geochim. Cosmochim. Acta 65, 387–406.
Aucour, A.M., Tao, F.X., Moreira-Turcq, P., Seyler, P., Sheppard, S., Benedetti, M.F., 2003. The Amazon River: behaviour of metals (Fe, Al, Mn) and dissolved organic matter in the initial mixing at the Rio Negro/Solimoes rivers confluence. Chem. Geol. 197, 271–285.
Auge, M., 2004. Regiones Hidrogeológicas. República Argentina, provincias de Buenos Aires, Mendoza y Santa Fe. Technical Report, 105 pp (La Plata).
Bonotto, D.M., 2006. Hydro(radio)chemical relationships in the giant Guarani aquifer, Brazil. J. Hydrol. 323, 353–386.
Bonotto, D.M., Caprioglio, L., 2002. Radon in groundwaters from Guarany aquifer, South America: environmental and exploration implications. Appl. Radiat. Isot. 57, 931–940.
Bouchez, J., Lajeneusse, J., Gaillardet, J., France-Lanord, C., Dutra-Maia, P., Maurice, L., 2010. Turbulent mixing in the Amazon River: the isotopic memory of confluences. Earth Planet. Sci. Lett. 290, 37–43.
Burnett, W.C., Dulaiova, H., 2003. Estimating the dynamics of groundwater input into the coastal zone via continuous radon-222 measurements. J. Environ. Radioact. 69, 21–35.
Burnett, W.C., Kim, G., Lane-Smith, D., 2001. A continuous radon monitor for assessment of radon in coastal ocean waters. J. Radioanal. Nucl. Chem. 249, 167–172.
Caplow, T., Schlosser, P., Ho, D.T., 2004. Tracer study of mixing and transport in the Upper Hudson River with multiple dams. J. Hydrol. Eng. 130, 1498–1500.
Cartwright, I., Hofmann, H., Sirianos, M.A., Weaver, T.R., Simmons, C.T., 2011. Geochemical and 222Rn constraints on baseflow to the Murray River, Australia, and timescales for the decay of low-salinity groundwater lenses. J. Hydrol. 405, 333–343.
Cey, E.E., Rudolph, D.L., Parkin, G.W., Aravena, R., 1998. Quantifying groundwater discharge to a small perennial stream in southern Ontario, Canada. J. Hydrol. 210, 21–37.
Cook, P.G., Favreau, G., Dighton, J.C., Tickell, S., 2003. Determining natural groundwater influx to a tropical river using radon, chlorofluorocarbons and ionic environmental tracers. J. Hydrol. 277, 74–88.
Craig, H., 1961. Isotopic variations in meteoric waters. Science 133, 1702–1703.
Depetris, P.J., Griffin, J.J., 1968. Suspended load in the Rio de la Plata drainage basin. Sedimentology 11, 53–60.
Depetris, P.J., Pasquini, A.I., 2007. The geochemistry of the Paraná River: an overview. In: Iriondo, M.H., Paggi, J.C., Parma, M.J. (Eds.), The Middle Paraná River: Limnology of a Subtropical Wetland. Springer, Berlin Heidelgerg, New York, pp. 143–174 (Chapter 6).
Diaz, E.L., Romero, E.C., Boschetti, N.G., Duarte, O.C., 2009. Vulnerabilidad del agua subterránea en la cuenca del Arroyo Feliciano, Entre Ríos, Argentina. Boletín Geológico y Minero 120 (4), 533–541.
Dimova, N.T., Burnett, W.C., Chanton, J.P., Corbett, J.E., 2013. Application of radon-222 to investigate groundwater discharge into small shallow lakes. J. Hydrol. 486, 112–122.
Donatti, L.M., Sawacuchi, A.O., Giannini, P.C., Fernandes, L.A., 2001. The Piramboia–Botucatu sucession (Late Permian–Early Cretaceous, Paraná Basin, Sao Paulo and Paraná States): Two contrasting eolian systems. Anais da Academia Brasileira de Ciencias 73 (3).
Drago, E.C., Amsler, M.L., 1988. Suspended sediment at a cross section of the Middle Parana River: concentration, granulometry and influence of the main tributaries. Sediment Budgets (Proceedings of the Porto Alegre Symposium, IAHS Publ. no. 174).
Drago, E.C., Vassallo, M., 1980. Campaña limnológica (Keratela I) en el río Paraná medio: características físicas y químicas del río y ambientes leníticos asociados. Ecol. Argentina 4, 45–54.
Dupré, B., Gaillardet, J., Rousseau, D., Allègre, C.J., 1996. Major and trace elements of river-borne material: the Congo Basin. Geochim. Cosmochim. Acta 60 (8), 1301–1321.
Eaton, A.D., Clesceri, L.S., Greenberg, A.E., 1995. Standard Methods for the Examination of Water and Wastewater. A.P.H.A./A.W.W.A./W.E.F., Washington D.C.
Elderfield, H., Upstili-Goddard, R., Sholkovitz, E.R., 1990. The rare earth elements in rivers, estuaries, and coastal seas and their significance to the composition of ocean waters. Geochim. Cosmochim. Acta 54, 971–991.
Facetti-Masulli, J.F., Klump, P., 2010. Selected minor and trace elements from water bodies of western Paraguay. J. Radioanal. Nucl. Chem. 286, 441–448.
Fernandes, L.A., Coimbra, A.M., 1996. A Bacia Bauru (Cretáceo Superior, Brasil). Anais da Academia Brasileira de Ciencias 68, 195–205.
Fernández-Caliani, J.C., Barba-Brioso, C., De La Rosa, J.D., 2009. Mobility and speciation of rare earth elements in acid minesoils and geochemical implications for river waters in the southwestern Iberian margin. Geoderna 149, 393–401.
Fili, M., 2001. Síntesis Geológica e Hidrogeológica del noroeste de la Provincia de Entre Ríos – República Argentina. Boletín Geológico y Minero 112, 25–36.

Gaillardet, J., Dupré, B., Allègre, C.J., Négrel, P., 1997. Chemical and physical denudation in the Amazon River Basin. Chem. Geol. 142, 141–173.
Gaillardet, J., Dupré, B., Louvat, P., Allègre, C.J., 1999. Global silicate weathering and $CO_2$ consumption rates deduced from the chemistry of large rivers. Chem. Geol. 159, 3–30.
García, M.G., Lecomte, K.L., Pasquini, A.I., Formica, S.M., Depetris, P.J., 2007. Sources of dissolved REE in mountainous streams draining granitic rocks, Sierras Pampeanas (Córdoba, Argentina). Geochim. Cosmochim. Acta 71, 5355–5368.
Garreaud, R.D., Vuille, M., Compagnucci, R., Marengo, J., 2008. Present-day South American climate. Palaeogeogr. Palaeoclimatol. Palaeoecol. 281, 180–195.
Gonfiantini, R., 1978. Standards for stable isotope measurements in natural compounds. Natura 271, 534–536.
Hamada, H., 1999. Analysis of the interaction between surface water and groundwater using Radon-222. Jpn. Agric. Res. Q. 33, 261–265.
Hamada, H., Imaizumi, M., Komae, T., 1997. Methods of investigation and analysis on ground-water using radon as an indicator. Nat. Res. Inst. Agric. Eng. 36, 17–50.
Hannigan, R.E., Sholkovitz, E.R., 2001. The development of middle rare earth element enrichments in freshwaters: weathering of phosphate minerals. Chem. Geol. 175, 495–508.
Ingri, J., Widerlund, A., Land, M., Gustafsson, O., Andersson, P., Ohlander, B., 2000. Temporal variations in the fractionation of the rare earth elements in a boreal river; the role of colloidal particles. Chem. Geol. 166, 23–45.
Iriondo, M., Praira, A., 2007. Physical Geography of the Basin. En Iriondo, M., Paggi, J., Parma, J., 2007. The Middle Paraná River – Limnology of a Subtropical Wetland. Berlin/Heidelberg, pp. 7–31.
Johannesson, K.H., Zhou, X., 1999. Origin of middle rare earth element enrichments in acid waters of a Canadian High Arctic lake. Geochim. Cosmochim. Acta 63, 153–165.
Johannesson, K.H., Tang, J.W., Daniels, J.M., Bounds, W.J., Burdige, D.J., 2004. Rare earth element concentrations and speciation in organic-rich blackwaters of the Great Dismal Swamp, Virginia, USA. Chem. Geol. 209, 271–294.
Kluge, T., von Rohden, C., Sonntag, P., Lorenz, S., Wieser, M., Aeschbach-Hertig, W., Ilmberger, J., 2012. Localising and quantifying groundwater inflow into lakes using high-precision $^{222}$Rn profiles. J. Hydrol. 450–451, 70–81.
Lambs, L., 2000. Correlation of conductivity and stable isotope $^{18}$O for the assessment of water origin in river system. Chem. Geol. 164, 161–170.
Lambs, L., 2004. Interactions between groundwater and surface water at river banks and the confluence of rivers. J. Hydrol. 288, 312–326.
Lane, S.N., Parsons, D.R., Best, J.L., Orfeo, O., Kostaschuk, R.A., Hardy, R.J., 2008. Causes of rapid mixing at a junction of two large rivers: Rio Paraná and Rio Paraguay, Argentina. J. Geophys. Res. 113 (F2).
Lee, D.R., 1977. Device for measuring seepage flux in lakes and estuaries. Limnol. Oceanogr. 648 (22), 140–147.
Leibundgut, C., Maloszewski, P., Külls, C., 2009. Tracers in Hydrology. Wiley-Blackwell JohnWiley & Sons, Chichester, UK.
Matsui, E., Salati, F., Friedman, I., Brinkman, W.L.F., 1976. Isotopic hydrology of the Amazonia: 2. Relative discharge of the Negro and Solimões rivers through $^{18}$O concentrations. Water Resour. Res. 12 (4), 781–785.
McBride, M.S., Pfannkuch, H.O., 1975. Distribution of seepage within lakebeds. J. Res. US Geol. Surv. 3, 505–512.
McLennan, S.M., 1989. Rare earth elements in sedimentary rocks: influence of provenance and sedimentary processes. In: Lipin, B.R., McKay, G.A. (Eds.), Geochemistry and Mineralogy of Rare Earth Elements, Reviews in Mineralogy 21. Mineralogical Society of America, Washington D.C., pp. 169–200.
McLennan, S.M., 2001. Relationships between the trace element composition of sedimentary rocks and upper continental crust. Geochem. Geophys. Geosyst. 2, 2000GC000109.
Meade, R.H., 1996. River-sediment inputs to major deltas. In: Milliman, J.D., Haq, B.U. (Eds.), Sea-level Rise and Coastal Subsidence: Causes, Consequences, and Strategies. Kluwer, Dordrecht, Cambridge, pp. 63–85.
Milani, E., Zalán, P., 1999. An outline of the geology and petroleum systems of the Paleozoic interior basins of South America. Episodes 22 (3), 199–205.
Milliman, J.D., Farnsworth, K.L., 2011. River Discharge to the Coastal Ocean. A Global Synthesis. Cambridge University.
Mullinger, N.J., Binley, A.M., Pates, J.M., Crook, N.P., 2007. Radon in chalk streams: Spatial and temporal variation of groundwater sources in the Pang and Laumbourn catchments, UK. J. Hydrol. 339, 172–182.
Orfeo, O., Iriondo, M.H., 2012. Variación quincenal de la concentración y tamaño de sólidos suspendidos del río Paraná (Corrientes, Argentina). Reunión de Comunicaciones Científicas y Tecnológicas, Universidad Nacional del Nordeste.
Orfeo, O., Stevaux, J., 2002. Hydraulic and morphological characteristics of middle and upper reaches of the Paraná River (Argentina and Brazil). Geomorphology 44, 309–322.
Panarello, H.O., Dapeña, C., 2009. Large scale meteorological phenomena, ENSO and ITCZ, define the Paraná River isotope composition. J. Hydrol. 365, 105–112.
Pasquini, A.I., Depetris, P.J., 2007. Discharge trends and flow dynamics of South American rivers draining the southern Atlantic seaboard: an overview. J. Hydrol. 333, 385–399.
Pasquini, A.I., Depetris, P.J., 2010. ENSO-triggered exceptional flooding in the Paraná River: where is the excess water coming from? J. Hydrol. 383, 186–193.
Pawellek, F., 1995. Geochemie und Isotopengeochemie von Flieβgewassern am Beispiel der oberen Donau und einiger ihrer Nebenflusse. RNDr thesis. Ruhr University, Bochum.
Peng, T.H., Takahashi, T., Broecker, W.S., 1974. Surface radon measurements in the North Pacific Ocean station Papa. J. Geophys. Res. 79 (12), 1772–1780.
Potter, P.E., 1978. Significance and origin of big rivers. J. Geol. 86, 13–33.
Ravenga, C., Murray, S., Abramovitz, J., Hammond, A., 1998. Watersheds of the World: Ecological Value and Vulnerability. World Resources Institute, Washington DC.
Santos, I., Niencheski, F., Burnett, W., Peterson, R., Chanton, J., Andrade, C., Milani, I., Schmidt, A., Knoeller, K., 2008. Tracing anthropogenically driven water discharge into a coastal lagoon from southern Brazil. J. Hydrol. 353, 275–293.
Sholkovitz, E.R., 1995. The aquatic chemistry of rare earth elements in rivers and estuaries. Aquat. Geochem. 1, 1–34.
Sholkovitz, E., Elderfield, H., Szymczak, R., Casey, K., 1999. Island weathering: river sources of rare earth elements to the western Pacific Ocean. Mar. Chem. 68, 39–57.
Smerdon, B.D., Gardner, W.P., Harrington, G.A., Tickell, S.J., 2012. Identifying the contribution of regional groundwater to the baseflow of a tropical river (Daly River, Australia). J. Hydrol. 464–465, 107–115.
Stringer, C.E., Burnett, W.C., 2004. Sample bottle design improvements for radon emanation analysis of natural waters. Health Phys. 87 (6), 642–646.
Tundisi, J.G., 1994. Tropical South America: present and perspectives. In: Margalef, R. (Ed.), Limnology Now: A Paradigm of Planetary Problems. Elsevier, Amsterdam, pp. 353–424.
Tweed, S.O., Weaver, T.R., Cartwright, I., Schaefer, B., 2006. Behavior of rare earth elements in groundwater during flow and mixing in fractures rock aquifers: an example from the Dandenong Ranges, southeast Australia. Chem. Geol. 234, 291–307.
Wang, H., Fu, R., 2004. Influence of cross-Andes flow on the South American low-level jet. J. Clim. 17, 1247–1262.
Yang, C., Telmer, K., Veizer, J., 1996. Chemical characteristics of the "St. Lawrence" riverine system: $\delta D_{H2O}$, $\delta^{13}C_{DIC}$, $\delta^{34}S_{sulfate}$ and dissolver $^{87}Sr/^{86}Sr$. Geochim. Cosmochim. Acta 60, 851–866.